Construction and Building Materials 216 (2019) 40–57

Contents lists available at ScienceDirect

Construction and Building Materials

journal homepage: www.elsevier.com/locate/conbuildmat

Prediction model of chloride diffusion in concrete considering the coupling effects of coarse aggregate and steel reinforcement exposed to marine tidal environment

Yuanzhan Wang [a], Xiaolong Gong [a,*], Linjian Wu [b]

[a] State Key Laboratory of Hydraulic Engineering Simulation and Safety and Collaborative Innovation Center for Advanced Ship and Deep-Sea Exploration, Tianjin University, 135 Yaguan Road, Jinnan District, Tianjin 300072, People's Republic of China

[b] National Engineering Research Center for Inland Waterway Regulation, School of River and Ocean Engineering, Chongqing Jiaotong University, 66 Xuefu Road, Nan'an District, Chongqing 400074, People's Republic of China

HIGHLIGHTS

- An in-door test for chloride diffusion under a real-time tidal cycle is carried out.
- Coupling effects of coarse aggregate (CA) and rebar on chloride diffusion is studied.
- Prediction model of chloride diffusion considering the CA and rebar is proposed.

ARTICLE INFO

Article history:
Received 14 November 2018
Received in revised form 18 April 2019
Accepted 25 April 2019
Available online 4 May 2019

Keywords:
Reinforced concrete
Chloride
Coarse aggregate and steel reinforcement
Coupling effects
Prediction model

ABSTRACT

Chloride-induced corrosion of steel reinforcement is one of the significant factors for the durability of the reinforced concrete structures exposed to marine environments. Reinforced concrete is a multiphase composite material composed of mortar, coarse aggregate, and rebar. The coarse aggregate and rebar can both affect the chloride diffusion characteristics of concrete. Nevertheless, the current researches related to the effects of the aforementioned two impact factors on chloride diffusion in concrete either considered the coarse aggregate only, or taken into account the steel bar separately. The coupling effects of coarse aggregate and steel reinforcement on chloride transport in concrete required to be further explored and discussed. In this paper, an in-door physical experiment for chloride diffusion in plain and reinforced concrete specimens exposed to marine tidal environment was carried out. The specimens were cast using different volume fractions of coarse aggregate and diameters of steel reinforcement. The chloride concentrations for experimental specimens were measured at various exposure times, and these measurements were adopted to further investigate the common influences of coarse aggregate volume fraction and blocking effect of rebar on chloride diffusion in concrete. Using the impact factors of coarse aggregate volume fraction $f(v)$, the direct and indirect blocking effect coefficients of rebar $\alpha(v)$, $\beta_r(\Phi/c)$ to improve the analytical solution of Fick's second law, a prediction model of chloride diffusion in concrete considering the coupling effects of coarse aggregate and steel reinforcement was proposed. The accuracy of this proposed prediction model was validated by comparing the chloride concentrations evaluated by the prediction model with the experimental measurements. The findings are expected to be useful in realistically predicting the durability of reinforced concrete structures.

1. Introduction

Chloride ions ingress in concrete is one of the most significant factors for reinforced concrete structures when exposed to marine environment, and this can cause the steel reinforcement corrosion, ultimately, shorten the durability and serviceability of reinforced concrete structures [1]. Therefore, it is essential to explore the transport behaviors of chloride ions in concrete covers and develop the useful chloride diffusion model in realistically predicting the durability of concrete structures [2].

Reinforced concrete is a multiphase composite material composed of mortar, coarse aggregate, and steel bar [3]. The coarse

* Corresponding author.
E-mail addresses: yzwang@tju.edu.cn (Y. Wang), gongxlomartin@163.com (X. Gong).

https://doi.org/10.1016/j.conbuildmat.2019.04.221
0950-0618/

aggregate is regarded as one of the vital components of concrete and they can significantly affect the chloride diffusion characteristics in concrete [4]. Some of the efforts devoted to study the effects of coarse aggregate on chloride migration in concrete. Yang and Cho [5] used the non-steady accelerate chloride migration test (ACMT) to inquire into the effect of lateral surface area of the regular cylindrical coarse aggregate on chloride diffusion coefficient of concrete specimens, and the chloride diffusion coefficients of interfacial transition zone (ITZ) were indirectly obtained. Yang [6] confirmed the volume fraction of coarse aggregate has significant influence on chloride diffusion coefficient through the ACMT. Shah et al. [7] proposed that the essential effects of coarse aggregate on chloride diffusion coefficient for concrete included dilution, tortuosity, and ITZ effects. Abyaneh et al. [8] developed a three-dimensional meso-scopic numerical model of concrete to investigate the effects of w/c; degree of hydration; volume fraction, size, shape and orientation of aggregate; width and percolation of ITZ on chloride diffusion coefficient for concrete using the finite element method (FEM). Li et al. [9] built three-dimensional concrete numerical model by Monte Carlo method and used the FEM to investigate the effects of shape, grading and volume fraction of aggregates; the thickness and permeability of ITZ on the effective permeability of chloride in concrete models. Wang et al. [10] proposed a time-and-depth-dependent chloride diffusion coefficient model (T-D model) for concrete considering the influences of coarse aggregate volume fraction (CAVF) and maximum size of aggregate (MSA). The T-D model can elaborate the variation characteristics for chloride diffusion coefficient of concrete with exposure time and diffusion depth varying. Wang et al. [11] investigated the effects of the heterogeneity of concrete materials (consistent with the influence of coarse aggregate) on long-term chloride diffusion in concrete using the meso-scopic FEM, and an empirical model for predicting long-term chloride profiles in concrete considering the various volume fractions of coarse aggregate was elaborated. Wang et al. [12] explored the effects of volume fraction and maximum size of natural coarse aggregate on chloride profiles and diffusion characteristics for concrete under drying-wetting cycles. A time-dependent model of surface chloride concentration and a multifactor model of chloride diffusion coefficient for concrete considering the exposure time, volume fraction and maximum size of natural coarse aggregate were developed.

Moreover, the blocking effects of steel reinforcement on chloride ions transport in reinforced concrete cannot be neglected as well. Actually, the accumulation phenomenon of chloride ions at the apex of rebar was reported by Hansen and Saouma [13] in 1999. Kranc and Sagues [14] pointed out that the blocking effect of rebar can enhance the chloride concentrations at the apex of steel reinforcement by numerical analysis, and they proposed the attenuation coefficient for chloride concentration due to the steel bar existence to explore the earlier initiation time of steel corrosion. Oh and Jang [15] used the FEM to estimate the chloride transport behaviors in reinforced concrete. They concluded that the larger diameter of rebar can result in greater accumulation of chloride concentrations at the apex of steel bar, as well as the initiation time of steel corrosion can shorten about 30–40% due to the reinforcement existence. The aforementioned literatures presented a convinced argument for the chloride accumulation at the apex of steel bar and a serious worry about the overestimating the service life of reinforced concrete structures, whereas few physical experiments for this problem were carried out. In this context, Wang et al. [16] tested the chloride concentrations at the apex of steel bar embedded in reinforced concrete members under the experimental drying-wetting cycles. The authors found the phenomenon of chloride accumulation in front of rebar, as well as the larger diameter of steel bars would result in greater chloride measurements. The direct and indirect blocking effects of the steel reinforcement were defined to reasonably describe the physical obstruction and the chloride diffusion coefficient variation due to the existence of cylindrical bar with various diameters.

Despite of all these laudable achievements during the previous investigations, however, the existing researches related to the effects of the coarse aggregate and steel reinforcement on chloride diffusion either considered the coarse aggregate volume fraction (or coarse aggregate content) only [5–12,17], or taken into account the blocking effect of steel bar separately [13–16]. The coupling effects of coarse aggregate and steel reinforcement on chloride diffusion in concrete required to be deeply researched and explored. In this paper, an in-door physical experiment for chloride diffusion in plain and reinforced concrete specimens exposed to marine tidal environment was carried out, and the specimens were cast using different volume fractions of coarse aggregate and diameters of steel reinforcement. The chloride concentrations for experimental specimens were measured at various exposure times, and they were used to investigate the common influence of volume fraction of coarse aggregate and blocking effect of rebar on chloride diffusion in concrete. Using the impact factors of coarse aggregate volume fraction, the direct and indirect blocking effect coefficients of steel bar to improve the analytical solution of Fick's second law, a prediction model of chloride diffusion in concrete considering the coupling effects of coarse aggregate and steel reinforcement was proposed. The accuracy of this proposed prediction model was validated through comparing the chloride concentrations evaluated by the prediction model with the experimental measurements.

2. Experimental studies

2.1. Materials and mixture proportions

During the experiment, the Ordinary Portland cement (P.O. 42.5) with the density of 3100 kg/m^3, which was produced by Tianjin Cement Plant, was used as the cementitious material for different experimental specimens. River sand with continuous grading, which can be considered as no initial chloride ions, was used as the fine aggregate, as well as the apparent density and fineness modulus for sand were 2610 kg/m^3 and 2.7, respectively. Natural crushed limestone with continuous grading was used as the coarse aggregate, in which its nominal size range and apparent density were 5–20 mm and 2690 kg/m^3. Distilled water was utilized during the process of experimental specimens casting, curing, and testing in order to avoid the interference of additional chloride ions within the raw materials on the final experimental measurements.

To explore the coupling effects of coarse aggregate volume fractions and diameters of steel bar on chloride diffusion characteristics of concrete, the mixture proportions for concrete specimens ($100 \times 100 \times 400$ mm^3) were designed by the standard [18]. The volume fractions of coarse aggregate $v = 0$, 0.2, 0.3, 0.4, and 0.5, and the details of mix proportions were listed in Table 1. The concrete can be generally simplified as a heterogeneous composite material consisting of three-phases, namely, cement paste, aggregate, and the interfacial transition zone (ITZ) at the meso-scale perspective [8]. In fact, the mortar can be also treated as a composite material consisting of cement paste, fine aggregate, and ITZ. However, the mortar is generally considered as a homogeneous chloride transport medium in concrete because of the smaller sizes of gel pores, capillary pores, and fine aggregates than those of coarse aggregate [19]. Therefore, the effect of aggregate on chloride diffusion in concrete is significantly attributed to the coarse aggregate. For this paper's study, the influence of fine aggregate on chloride diffusivity can be reasonably neglected. The hot-rolled plain round steel bars (HPB300) with diameters of $\Phi = 0$, 8, 12, 16, and 20 mm were used and embedded in experimental specimens. The detail

Table 1
Mixtures details for concrete specimens with various volume fractions of coarse aggregate.

w/c	Cement (kg/m^3)	Water (kg/m^3)	Fine aggregate (kg/m^3)	Coarse aggregate (kg/m^3)	volume fraction of coarse aggregate, v
0.54	345	639	1173	0	0
	277	512	932	538	0.2
	242	448	816	807	0.3
	208	384	699	1076	0.4
	173	320	583	1345	0.5

information of the steel bar properties were provided in Table 2. The experimental specimens with $\Phi = 0$ mm means there is no steel bar installed in concrete, and these types were named as the plain concrete specimens. Also, the others with $\Phi \neq 0$ mm were called as the reinforced concrete specimens. To sum up, during this paper's experiment, the numbers of coarse aggregate volume fractions and steel bar diameters are both 5, namely, the total experimental groups are equal to 25, as exhibited in Table 3.

2.2. Casting, curing and preparation for specimens

Plain and reinforced concrete specimens, all measuring $100 \times 100 \times 400$ mm^3 sizes and considering the concrete cover of 20 mm for reinforced concrete, were cast in plastic molds, subsequently, compacted on a vibrating table. After casting for 24 h kept temperature of 20 ± 3 °C and over 90% relative humidity, experimental specimens were demoded and moved to water saturated with $Ca(OH)_2$ at 20 ± 3 °C for 28 days curing. Then, all the specimens were sealed on the five sides using epoxy polyurethane based coating to expose only one side (100×400 mm^2) to make sure chloride ions would diffuse only in one-dimension.

For this paper's study, the slump values (S_v) of three mixture proportions of concrete with $v = 0.3$, 0.4, and 0.5 were measured to evaluate the effect of coarse aggregate on the workability and rheological properties of fresh concrete. They were determined as $S_v(v = 0.3) = 131$ mm, $S_v(v = 0.4) = 123$ mm, and $S_v(v = 0.5) = 115$ mm per the procedure of GB 50164-2011 [20]. An increase in design volume fraction of coarse aggregate from $v = 0.3$ to 0.5 resulted in a lower slump, and the slump values decreased from 131 to 115 mm, representing a 13.9 % reduction, when the coarse aggregate volume fraction was increased from 0.3 to 0.5. This is due to lower cement paste content in concrete mixes, providing less lubrication for the coarse aggregates and reduced workability. In addition, the compressive strength results of 28 days (f_c) for the aforementioned three uniform mixture proportions of concrete are tested based on three specimens and their average results are $f_c(v = 0.3) = 38.3$ MPa, $f_c(v = 0.4) = 46.4$ MPa and $f_c(v = 0.5) = 53.2$ MPa. The 28 days compressive strength increased with the volume fraction of coarse aggregate increasing. This indicated that the increased coarse aggregate volume fractions led to compressive strength of concrete improvement, which is consistent with the reality.

2.3. Exposure environment

To simulate the marine environment in diurnal tidal zone, the artificial marine tidal environment automatic simulation device, which developed by the research team of Harbour Engineering Structure Laboratory in Tianjin University, is used to realistically simulate the real-time tidal cycles. This device contained a series of components including the test tank, storage tank (water level indicator), flow rate control system (flow meter, water pump, and solenoid value, etc.), air-blast system, temperature control system, humidity control system, spray system (sprayer, sprinkler), operating system, etc., which connected with each others based on the programmable logic controller (PLC), shown in Fig. 1. Comparing to the totally wet and totally dry conditions in traditional wetting-drying cycles [10,12,16,17], this device can automatically, effectively and realistically simulate the real-time rising and ebb tide cycling simulation during the long-term test periods, which is more approximated to the true circumstance. Some significant controlling parameters, for instance the number of tidal cycles, the high- and low-water level values, the temperature and relative humidity in test tank, etc., can be set through the parameters input interface of operating system, and the automatic simulation device would complete the requested action by receiving the command from the programs compiled into the PLC controller. This device can not only control the water level to go up and down gradually in marine tidal zone but also adjust the temperature, relative humidity, and other ocean environmental impact factors, which realized the test automation and greatly improved the experimental efficiency. 3.5% sodium chloride solution was configured and used as the seawater, and all experimental specimens were vertically placed on a corrosion-resistant table (200 mm high) located in test box of this device for chloride ions diffusion. In terms of the geometric sizes of the specimens, the high and low tidal levels were set as 600 ± 20 mm and 200 ± 20 mm respectively. The tidal cycle period was 24 hours (one day), including 12 hours for rising

Table 2
Properties of steel bar.

Type	Eigenvalue	d_r (mm)	$d_{r(m)}$ (mm)	Weight (kg/m)	R_{el} (MPa)	R_m (MPa)	A (%)	A_{gt} (%)
HPB300	Max	8	8.24	0.416	390	515	39.5	22.5
		12	12.18	0.919				
		16	16.32	1.613				
		20	20.24	2.574				
	Min	8	7.92	0.385	335	460	31.5	16
		12	11.86	0.841				
		16	15.76	1.526				
		20	19.82	2.430				
	Average	8	8.08	0.401	362.5	487.5	35.5	19.3
		12	12.02	0.880				
		16	16.04	1.570				
		20	20.03	2.502				

d_r and $d_{r(m)}$ denote the theoretical diameter and the measured diameter of rebar; R_{el} and R_m mean the yield strength and the tensile strength of rebar, respectively; A and A_{gt} are the fracture elongation and the elongation at maximum load, respectively.

Table 3
Codes of plain and reinforced concrete specimens.

Code		Diameters of rebar, Φ (mm)				
		0	8	12	16	20
Volume fractions of coarse aggregate, v	0	Φ0-0	Φ8-0	Φ12-0	Φ16-0	Φ20-0
	0.2	Φ0-0.2	Φ8-0.2	Φ12-0.2	Φ16-0.2	Φ20-0.2
	0.3	Φ0-0.3	Φ8-0.3	Φ12-0.3	Φ16-0.3	Φ20-0.3
	0.4	Φ0-0.4	Φ8-0.4	Φ12-0.4	Φ16-0.4	Φ20-0.4
	0.5	Φ0-0.5	Φ8-0.5	Φ12-0.5	Φ16-0.5	Φ20-0.5

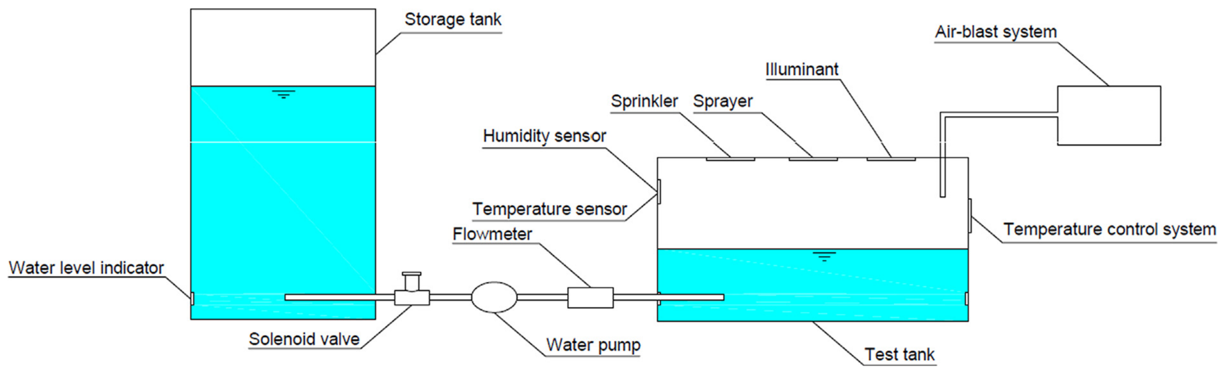

Fig. 1. Artificial marine environment automatic simulation device.

tide and other 12 hours for ebb tide. The exposure times for experimental specimens of Φ = 0 mm (no rebar existence) were 30, 70, 100, 140, and 180 consecutive days, as well as for the specimens of Φ = 8, 12, 16, and 20 mm were 100, 140, and 180 consecutive days, respectively.

2.4. Samples and testing

The real-time tidal cycles can significantly affect the chloride ions distributions along the elevation direction of concrete structures. According to an in-site test for a certain wharf concrete structure, the tested chloride concentration results decreased with the structural elevation increasing, and the most unfavorable chloride concentrations were distributed at the areas about 1/4–1/2 elevation from the bottom of the structure (the midway down of the wharf structure) [21]. On the basis of the aforementioned summary, after each required chloride exposure time completed, the related experimental specimens were taken out of the device's test box and were averagely divided into four parts numbered ①–④ from the bottom to the top, and the part ② was used as the representative to drill the concrete powders, as shown in Fig. 2. To make sure the test accuracy, the concrete cubes of part ② were again divided into two parts (see in Fig. 2), and the powders for the two parts in any of the same holes were respectively drilled and obtained. The chloride concentrations were measured using the two powders which obtained in same sample holes, and the average values of the two were treated as the final chloride ion results in this hole position. In addition, all the powders obtained were dried for 2 h in the drying box (105 ± 5 °C) after being sieved through the sieve with a 0.63 mm aperture, subsequently, they were separately tested to determine the water-soluble chloride concentration (free chloride) at each depth by the standard [22].

3. Results analysis and model establishment

3.1. Tested results

(1) Chloride profiles in plain concrete specimens (Φ = 0 mm)

For the plain concrete specimens (denotes the diameter of steel bar Φ = 0 mm), the tested chloride profiles against diffusion depths in concrete specimens with various volume fractions of coarse aggregate at different exposure times are exhibited in Fig. 3. The free chloride concentration results shown in Fig. 3 and the following figures for this paper's study are all presented as a percentage of the concrete mass (%). The chloride concentrations in concrete specimens with various coarse aggregate volume fractions, as expected, increase with the exposed time increasing, whereas decrease with the diffusion depth increasing. These variation trends for chloride profiles are consistence with the results reported in literatures [5,11,12,16,17].

(2) Chloride concentration distributions in reinforced concrete specimens (Φ ≠ 0 mm)

The chloride concentration distributions within the reinforced concrete specimens with different diameters of Φ = 8, 12, 16, and 20 mm are all measured during the experiment procedure. A representative, in which the volume fraction of coarse aggregate, diameter of rebar and exposure time are v = 0.2, Φ = 12 mm and t = 180 d respectively, is used to exhibit the tested chloride concentration isolines, as shown in Fig. 4. The data involved in Fig. 3 present the chloride concentration values located on various isolines. Fig. 4 illustrates that the phenomenon of chloride accumulation is occurred at the apex of rebar, and the impact region is about 3–5 mm from the apex of rebar to the exposure surface of reinforced concrete specimen. Moreover, the chloride concentrations are tended to be consistence in a same diffusion depth (sample holes in an uniform x coordinate with various y coordinates) with the distance from the apex of rebar increasing. Thus, it means that the steel reinforcement embedded in concrete can significantly affect the chloride ion concentration distributions around the rebar.

3.2. Prediction model of chloride profiles considering the effect of coarse aggregate

When the reinforced concrete structures are exposed to the marine aggressive environments, the chloride ions can ingress in

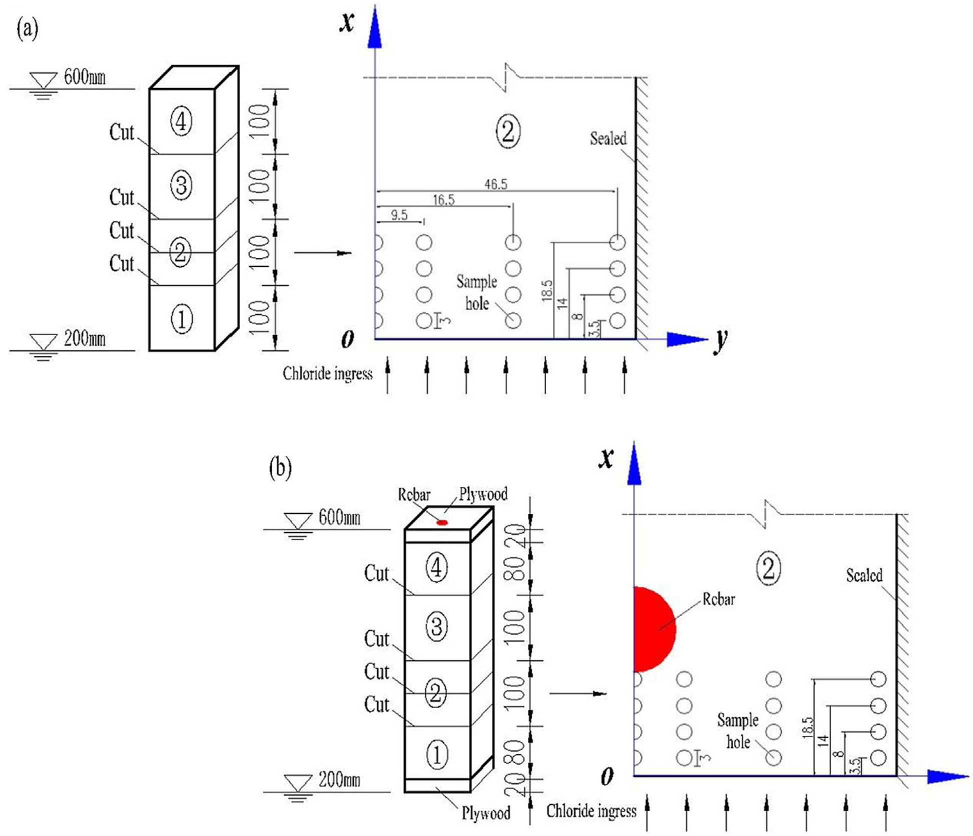

Fig. 2. Specimens processed and sample holes distribution for (a) plain concrete; (b) reinforced concrete (units: mm).

concrete through multiple mechanisms, such as diffusion, convection, adsorption, permeation and surface deposit of airborne salts. However, among these reasons, the main transport mechanism for chloride ions in concrete is diffusion [23,24], which can be modeled using Fick's second law of diffusion:

$$\frac{\partial C}{\partial t} = \frac{\partial C}{\partial x}\left(D \cdot \frac{\partial C}{\partial x}\right) \tag{1}$$

where C denotes chloride concentration (%); D means chloride diffusion coefficient of concrete (m^2/s); t is exposure time (s); x denotes the diffusion depth (m). According to a large number of investigations, the boundary condition of $C = C_s$ (for $x = 0,\ t \geq 0$) and the chloride diffusion coefficient D should be both considered as time-dependent parameters resulting in $C_s = C_s(t)$ and $D = D(t)$ [25], where C_s means the surface chloride concentration (%). Formulas of $C_s(t)$ can be expressed as linear, square-root, power, exponent, and logarithmic functions [11]. Also, the time-dependency of chloride diffusion coefficient $D(t)$ is more appropriately modeled based on a power function proposed by Thomas and Bamforth [26] as follows:

$$D(t) = D_{28}\left(\frac{t_{28}}{t}\right)^m \tag{2}$$

where $D(t)$ means the chloride diffusion coefficient at the exposure time t (m^2/s); D_{28} denotes the chloride diffusion coefficient at the exposure time $t = 28$ d (m^2/s), and D_{28} can be also defined as the reference chloride diffusion coefficient; m is the aging factor. Substituting the Eq. (2) and $C_s = C_s(t)$ into Eq. (1) and considering the actual initial condition $C = C_0$ (for $x > 0,\ t = 0$) (where C_0 denotes the initial chloride concentration of concrete before exposure to the marine environment (%)), the solution of Eq. (1) considering the time-dependency of the chloride diffusion coefficient and the surface chloride concentration is determined as:

$$\begin{cases} C(x,t) = C_s(t)\left[1 - \mathrm{erf}\left(\frac{x}{2\sqrt{D_a(t)\cdot t}}\right)\right] \\ D_a(t) = \frac{D_{28}}{1-m}\left(\frac{t_{28}}{t}\right)^m \end{cases} \tag{3}$$

where D_a denotes the apparent chloride diffusion coefficient (m^2/s). D_a is also a time-dependent parameter, $D_a = D_a(t)$ [27–30], and the expression form of $D_a(t)$ can be based on the references [31,32]; erf(·) is the error function. The significant parameters $C_s(t)$, $D_a(t)$, D_{28} and m within Eq. (3) can be determined by fitting the experimental measurements using a non-linear regression analysis based on the method of least squares fit.

(1) Surface chloride concentration $C_s(t)$

The surface chloride concentrations C_s for different plain concrete specimens with $v = 0$, 0.2, 0.3, 0.4 and 0.5 at various exposure times are determined by fitting the Fick's second law of diffusion to the corresponding tested chloride profiles (see in Fig. 3) using regression analysis. Fig. 5 plots the values of surface chloride concentration with various volume fractions of coarse aggregate at different exposure times. Also, this figure depicts that the surface chloride concentration scatters increase with the exposure time increasing, validating the time-dependency of surface chloride concentration. Moreover, although the surface chloride concentrations at each time exhibit random fluctuation with coarse aggregate volume fraction varying, the little differences between the scatters and their average values are shown in Fig. 5. Thus, it is appropriate to consider that the surface chloride concentrations are independent of volume fraction of coarse aggregate, namely,

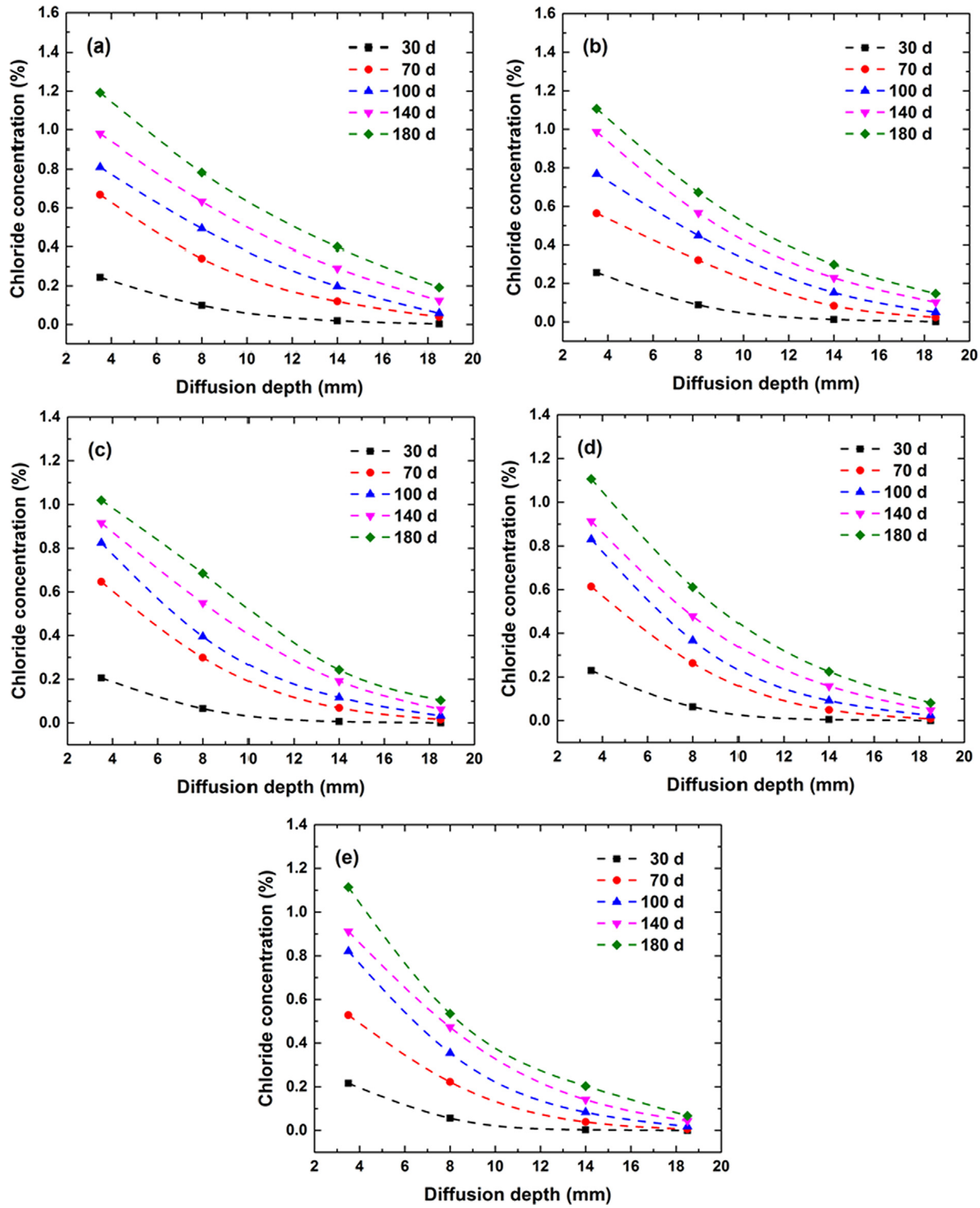

Fig. 3. Chloride profiles for concrete specimens with various volume factions of coarse aggregate: (a) $v = 0$; (b) $v = 0.2$; (c) $v = 0.3$; (d) $v = 0.4$; (e) $v = 0.5$.

there is no specific relation between surface chloride concentration and coarse aggregate. Fitted formula of surface chloride concentration against the exposure time, $C_s(t)$, can be reasonably quantified as logarithmic functions [33] for this paper's C_s scatters, and the fitted curve and expression are hence expressed in Eq. (4) and shown in Fig. 5, respectively.

$$C_s(t) = 0.6009 \cdot \ln(t) - 1.6192, \ t \geq 30 \text{ d} \tag{4}$$

(2) Apparent chloride diffusion coefficient D_a, reference chloride diffusion coefficient D_{28} and aging factor m

The apparent chloride diffusion coefficients D_a for different plain concrete specimens with $v = 0$, 0.2, 0.3, 0.4, and 0.5 at various exposure times can be simultaneously confirmed by fitting the Fick's second law of diffusion to the corresponding tested chloride profiles (see in Fig. 3) using regression analysis. Fig. 6 illustrates

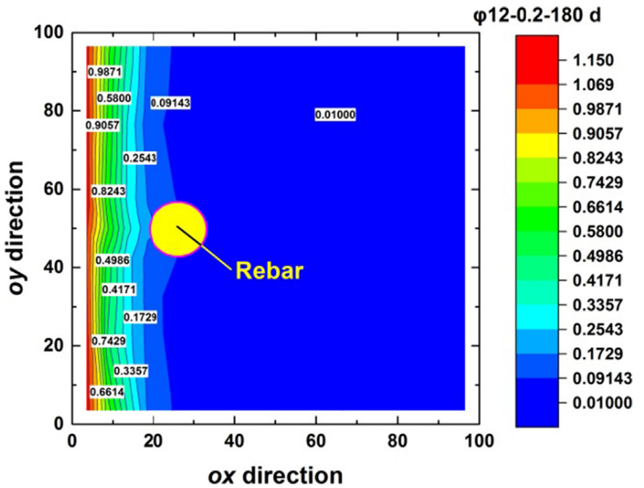

Fig. 4. Chloride concentration distribution of reinforced concrete specimens with $\Phi = 12$ and $v = 0.2$ at $t = 180$ d.

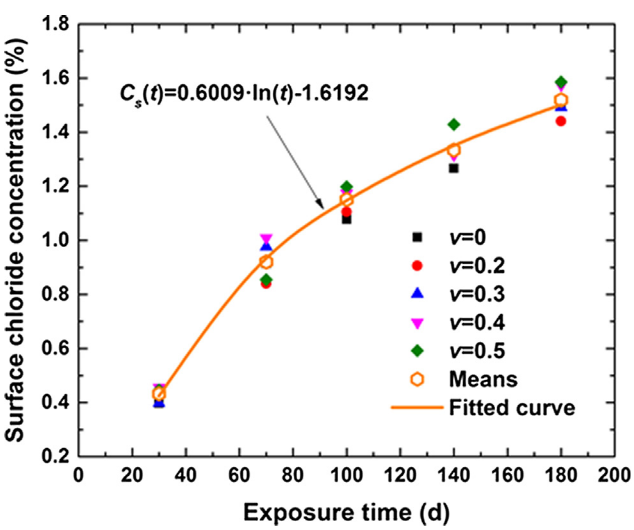

Fig. 5. Surface chloride concentrations versus exposure time $C_s(t)$.

the apparent chloride diffusion coefficients with different volume fractions of coarse aggregate over the exposure time. From this figure, we can obtained that the apparent chloride diffusion coefficients all decrease with exposure time and coarse aggregate volume fraction increasing. Subsequently, the reference chloride coefficient D_{28} and aging factor m with different volume fraction of coarse aggregate (v = 0, 0.2, 0.3, 0.4, and 0.5) are simultaneously determined by fitting the $D_a(t) = \frac{D_{28}}{1-m}\left(\frac{t_{28}}{t}\right)^m$ (the second formula in Eq. (3)) to the D_a scatters using the regression analysis. The results of D_{28} are marked in Fig. 6 and the m values are shown in Fig. 7. The variation trend of D_{28} versus coarse aggregate volume fractions are consist with D_a that the reference chloride diffusion coefficient D_{28} decrease with the volume fraction of coarse aggregate increasing. Additionally, the scatters of aging factor m present random fluctuation with volume fraction of coarse aggregate varying, as well as the little differences between the m scatters and their average values are shown in Fig. 7. Consequently, it is reasonable to confirm that there is no specific relation between the aging factor and the coarse aggregate volume fraction of concrete, and the average value $m = 0.333$ is considered as the aging factor in Eq. (3).

(3) Impact factor of coarse aggregate volume fraction $f(v)$

To quantify the effect of coarse aggregate volume fraction on chloride diffusion coefficient, the impact factor of coarse aggregate volume fraction $f(v)$ is defined as:

$$f(v) = \frac{D_{28}(v)}{D_0} \tag{5}$$

where $D_{28}(v)$ denotes the reference chloride diffusion coefficient for plain concrete specimens with v = 0, 0.2, 0.3, 0.4, and 0.5, and their results are shown in Fig. 6; D_0 is the reference chloride diffusion coefficient when $v = 0$, $D_0 = D_{28}(v = 0) = 6.42 \times 10{-}12\ \mathrm{m^2/s}$. The scatters for $f(v)$ are calculated in accordance with Eq. (5) and are plotted in Fig. 8. Using the linear function to fit the $f(v)$ values, the fitted curve and formula are shown in Fig. 8 and expressed as follows:

$$f(v) = 1 - 1.0182v \tag{6}$$

(4) Prediction model establishment and verification

Inserting the time-dependent surface chloride concentration $C_s(t) = 0.6009 \cdot \ln(t) - 1.6192$, the reference chloride diffusion coefficient $D_{28}(v) = D_0 \cdot f(v)$ and the aging factor $m = 0.333$ into Eq. (3), the

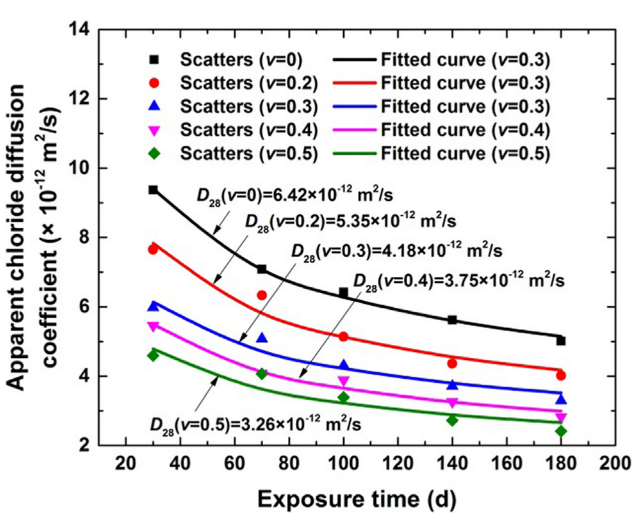

Fig. 6. Apparent chloride diffusion coefficients versus exposure time.

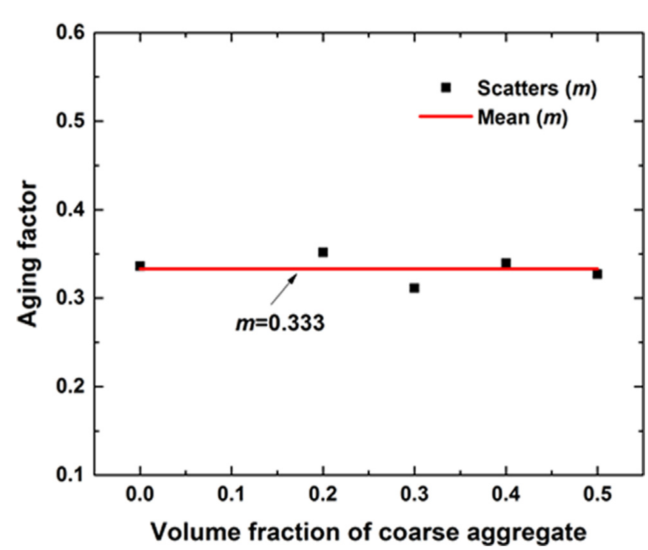

Fig. 7. Aging factors versus volume fraction of coarse aggregate.

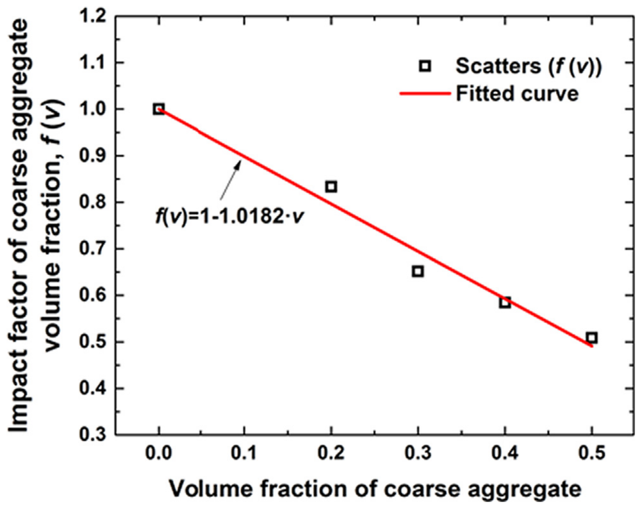

Fig. 8. Impact factors of coarse aggregate volume fraction $f(v)$ and its fitted curve.

prediction model of chloride profiles considering the effect of coarse aggregate volume fraction is established as:

$$\begin{cases} C(x,t,v) = C_s(t)\cdot\left[1-\mathrm{erf}\left(\frac{x}{2\sqrt{\frac{D_{28}(v)}{1-m}\left(\frac{t_{28}}{t}\right)^m t}}\right)\right] \\ C_s(t) = 0.6009\cdot\ln(t) - 1.6192 \\ D_{28}(v) = f(v)\cdot D_0, \quad f(v) = 1-1.0182\cdot v \\ D_0 = 6.42\times10^{-12}\mathrm{m}^2/\mathrm{s}, \quad m = 0.333 \end{cases} \tag{7}$$

the prediction model of Eq. (7) proposed by this paper can be used to rapidly, high-efficiently and conveniently determine the chloride diffusion concentration profiles in concrete specimens with different volume fractions of coarse aggregate at arbitrary exposure time or depth. The variables including diffusion depths x, exposure times t, and the volume fractions of coarse aggregate v, which are consistent with the experimental study, for example x = 3.5, 8, 14, 18.5 mm; t = 30, 70, 100, 140, and 180 d; v = 0, 0.2, 0.3, 0.4, 0.5, are inserted in Eq. (7). Subsequently, the corresponding chloride concentration results can be calculated in terms of Eq. (7) and applied to compare with the experimental chloride measurements in Fig. 3, as shown in Fig. 9. Fig. 9 depicts the trend variations of chloride concentrations in different plain concrete specimens against the depths and exposure times. The chloride concentrations, no matter the experimental results or the predicted values by Eq. (7), both decrease as the diffusion depth increases, whereas increase with the exposure times increasing. This is consistent with the actual situation. The magnitudes of the chloride concentrations evaluated by prediction model Eq. (7) are in good agreement with those from the experiments. Moreover, the chloride results for various plain concrete specimens predicted based on the model Eq. (7) against the experimental measurements are plotted in Fig. 10. The chloride concentration data in Fig. 10 all come from Fig. 9. The experimental chloride concentration results of concrete with different volume fractions of coarse aggregate (scatters in Fig. 9) are treated as the abscissa in Fig. 10, and the chloride results determined by the prediction model Eq. (7) (curves in Fig. 9) are regarded as the ordinate in Fig. 10. Fig. 10 can intuitively show and analyze the relative errors between the predicted chloride concentrations by Eq. (7) and the chloride results tested by experiment, and this method can refer to references [31,34]. This figure shows that almost all of the chloride concentrations estimated by prediction model Eq. (7) are located within a ±15% error margin, validating the accuracy and reliability of the prediction model for plain concrete specimens developed in this paper. Additionally, the chloride diffusion coefficients from the experiment and the predicted model Eq. (7) are also listed in Table 4. The chloride diffusion coefficients determined by Eq. (7) show good correlation with those of experiment, and the relative errors between the both chloride diffusion coefficients are almost within a ±10% margin, further validating the accuracy and reliability of the prediction model proposed by this paper. In sum, the prediction model of chloride diffusion in concrete considering the effect of coarse aggregate volume fraction (Eq. (7)) can accurately predict the chloride concentration profiles and diffusion characteristics for plain concrete.

3.3. Prediction model of chloride concentration considering the coupling effects of coarse aggregate and steel reinforcement

To further explore the effect of steel reinforcement with different diameters on chloride diffusion concentration in concrete with various coarse aggregate volume fractions, the tested chloride concentrations at the apex of rebar (coordinate x = 18.5 mm and y = 0 mm shown in Fig. 2) for the reinforced concrete specimens, which included the diameters of rebar Φ = 0, 8, 12, 16, 20 mm; the volume fractions of coarse aggregate v = 0, 0.2, 0.4; and the experimental exposure times t = 100, 140, 180 d, are all plotted in Fig. 11. In this figure, we can observe that the chloride concentrations at the apex of rebar with Φ = 8, 12, 16, 20 mm are all greater than those of Φ = 0 mm when the volume fraction of coarse aggregate is constant, and the difference of chloride concentrations between the rebar diameter Φ = 8, 12, 16, 20 mm and Φ = 0 mm increases with the diameter increasing. Subsequently, the chloride results at the apex of rebar with Φ = 8, 12, 16, 20 mm against the values for Φ = 0 mm are drawn in Fig. 12. Figs. 11 and 12 both indicate that the blocking effect of steel bar existence can significant enhance the chloride concentrations at the surface of rebar, and the chloride ion concentrations at the apex of rebar are approximate to maximum three times than those of no rebar. To sum up, it is necessary to deeply explore and further quantify the blocking effect of steel reinforcement on chloride diffusion concentration in concrete with different volume fractions of coarse aggregate, especially, at the place of rebar apex.

Wang et al. [16] reported that the blocking effect of rebar existence on chloride concentration distribution in concrete is divided into two part, i.e. indirect blocking effect and direct blocking effect. The followings will respectively elaborate the influence of indirect and direct blocking effects on chloride concentration at the apex of rebar.

(1) Determination for coarse aggregate content in front of the steel bar

The steel reinforcement embedded in concrete can alter the mesoscopic structure of concrete adjacent to the rebar, i.e. update the coarse aggregate content and distribution within a certain area around the steel reinforcement, thereby, affect the chloride diffusion coefficient at this area in front of the rebar. This physical phenomenon is defined as the indirect blocking effect of steel bar [35,36].

The three reinforced concrete specimens with Φ = 16 mm at the exposure time of 100, 140, and 180 d are treated as the representatives, and the part ③ and ④ of the three samples (shown in Fig. 2 (b)) are further divided into two parts along the axle wire of rebar, as exhibited in Fig. 13(a). Subsequently, the particle image instrument and its corresponding devices is adopted to scan the sections of reinforced concrete (S_1, S_2 marked in Fig. 13(a)), and then, to quantify the coarse aggregate contents and distribution in front

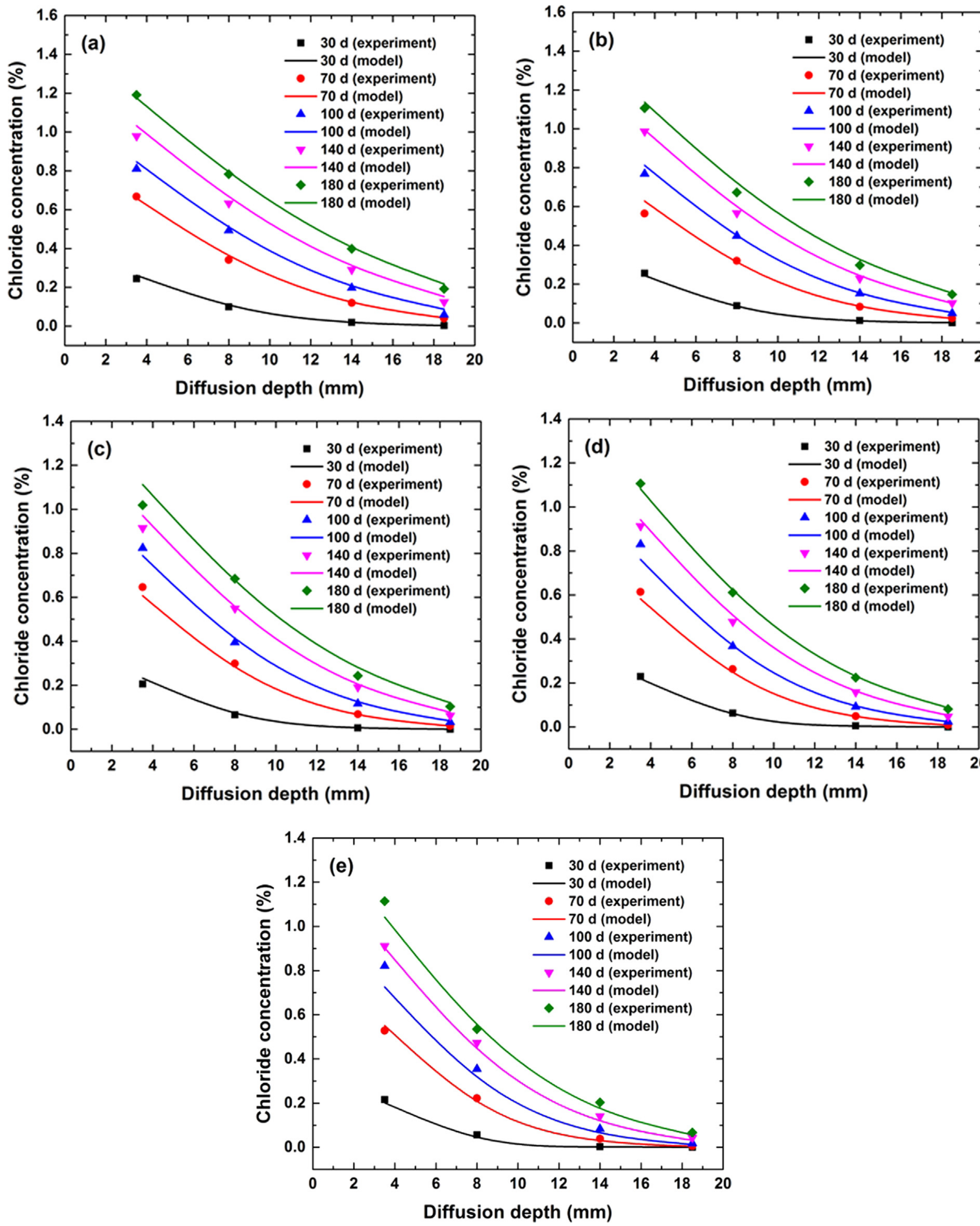

Fig. 9. Comparison of the chloride profiles of concrete specimens between the experiment and prediction model Eq. (7): (a) $v = 0$; (b) $v = 0.2$; (c) $v = 0.3$; (d) $v = 0.4$; (e) $v = 0.5$.

of the rebar. The device mainly consists of three components, including the particle image instrument, main controller and computer, as shown in Fig. 14. The test implementation procedures are expressed as follows:

1) The high resolution images for the sections of reinforced concrete samples require to be obtained using the scanning function of the particle image instrument, and an instance is shown in Fig. 13(b).
2) The real and high resolution images for reinforced concrete samples need to be further processed in black and white, as shown in Fig. 13(c).
3) The concrete cover within the black and white images are evenly divided into 1 mm/layer, and the area fractions of coarse aggregate in each area ($1 \times 100\ mm^2$ rectangle), i.e. the percentage of the white region (denotes coarse aggregate) accounting for the $1 \times 100\ mm^2$ rectangle exhibited in Fig. 13(c), are determined respectively.

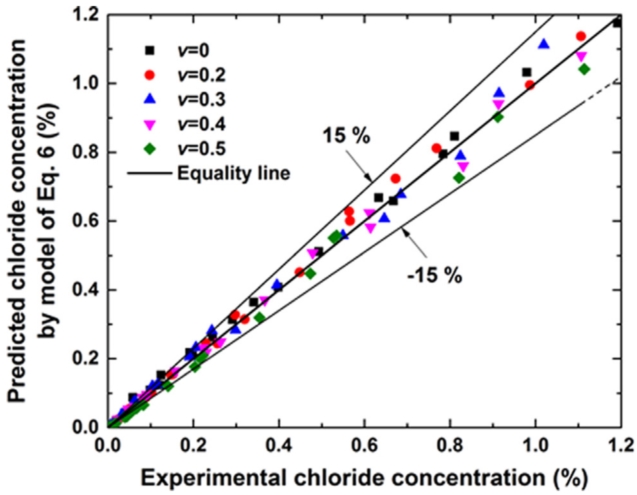

Fig. 10. Comparison of the chloride concentrations by the prediction model Eq. (7) versus those of experiment in concrete specimens with different volume fractions of coarse aggregate.

The area fractions of coarse aggregate Arc in different divided areas ($1 \times 100\,mm^2$ rectangle) along the front of steel bar ($\Phi = 16$ mm) for reinforced concrete sections with their original coarse aggregate volume fractions $\upsilon = 0.2$, 0.3, 0.4, and 0.5 are respectively determined during the aforementioned procedures. The results are shown in Fig. 13(d). Fig. 13(d) depicts that the area fractions of coarse aggregate A_{rc} at the adjacent region of steel bar show lower than their corresponding original coarse aggregate volume fractions, i.e. $A_{rc} < v$, and the area fractions of coarse aggregate A_{rc} initially increase and then tend to stable with the distance along the front of rebar increasing. The increased A_{rc} is included in approximately 4 mm width region along the apex of rebar, whereas the values of A_{rc} tend to constant when the distance exceeds 4 mm. Consequently, it is reasonable to consider that the influence area of steel reinforcement ($\Phi = 16$ mm) on coarse aggregate distribution around the steel bar is about $4 \times 100\,mm^2$ in close proximity to the rebar, and this result is very similar to the conclusion reported in literature [35]. Subsequently, the particle image instrument is again used to measure the total area fractions of coarse aggregate $A_{rc(t)}(\upsilon)$ in the rectangle of $4 \times 100\,mm^2$ next to the steel bar ($\Phi = 16$ mm) for different reinforced concrete sections. The original coarse aggregate volume fractions of these sections are equal to $\upsilon = 0.2$, 0.3, 0.4, and 0.5, as shown in Fig. 13(e). Notice that the value of $A_{rc}(t)$ with each volume fraction of coarse aggregate υ is determined by the average values of three reinforced concrete samples' measurements, and the three samples are corresponding with the exposure times of 100, 140, and 180 d.

To compare the $A_{rc(t)}(\upsilon)$ with the total area fraction of coarse aggregate at the consistent influence region of steel reinforcement for their corresponding plain concrete sections (no rebar, $\Phi = 0$ mm), the particle image instrument is re-applied to test the total area fractions of coarse aggregate $A_{pc}(\upsilon)$ in the same $4 \times 100\,mm^2$ rectangle of plain concrete samples during the implementation procedures of Fig. 15.

Drawing the whole measured $A_{rc}(t)$ and A_{pc} scatters and their corresponding average values against the volume fractions of coarse aggregate in Fig. 16, and we can observe that:

1) The tested $A_{rc}(t)$ and A_{pc} scatters, in which are corresponding to the diameter of steel bar $\Phi = 16$ mm and $\Phi = 0$ mm (no rebar), respectively, have little differences with each other on the precondition of a consistent volume fraction of coarse aggregate. Moreover, the relative errors between the scatters and their average values are all within ±15% range. Accordingly, it's appropriate to consider that the average values of $A_{rc}(t)$ and A_{pc} at each coarse aggregate volume fraction can be as the representative during the following analysis.
2) The average values of $A_{rc}(t)$ are all lower than the original volume fractions of coarse aggregate υ within reinforced concrete specimens (see in Fig. 16(a)), validating that the rebar existence can decrease the content of coarse aggregate in a certain region around the steel reinforcement, and then, increase the chloride diffusion coefficient in this region, thus, enhance the chloride ion concentration at the surface of rebar. This indicates the essential mechanism for the indirect blocking effect of steel bar.
3) The tested average values of A_{pc} are approximately equal to the original volume fractions of coarse aggregate υ for reinforced concrete specimens, as shown in Fig. 16(b) (the abscissa in Fig. 16(b) denotes the actual volume fractions of coarse aggregate υ, and the ordinate means the tested A_{pc} values). For the aforementioned phenomenon, Zheng et al. [37] numerically simulate the distribution of aggregate particles at a concrete element considering the effect of formwork walls. The simulation results show that the volume fraction of average aggregate initially increased and then asymptotically trended to a certain value as the depth from the surface to the inside of concrete element increasing. Moreover, the stable aggregate volume fraction values are approach to the area fraction of aggregate [38,39]. During this paper's scanning experiment, the conclusion is in accord with the references [37,38,39]. Accordingly, for this paper's study, it can be reasonable to consider $A_{pc} = \upsilon$.

(2) Indirect blocking effect coefficient of rebar α

To quantify the influence of indirect blocking effect of rebar on chloride diffusion coefficient at the apex of steel bar, the indirect blocking effect coefficient of rebar α considering the volume fraction of coarse aggregate υ is hence defined as:

$$\alpha(\upsilon) = \frac{D_{28}(A_{rc(t)})}{D_{28}(A_{pc})} = \frac{D_{28}(A_{rc(t)})}{D_{28}(\upsilon)} = \frac{D_0 \cdot f(A_{rc(t)})}{D_0 \cdot f(\upsilon)} = \frac{1 - 1.0182 \cdot A_{rc(t)}}{1 - 1.0182 \cdot \upsilon} \tag{8}$$

Table 4
Chloride diffusion coefficient from the experimental result and the predicted model.

v / t	0			0.2			0.3			0.4			0.5		
	ER	PM	RE	ER	PM	RE	ER	PM	RE	ER	PM	RE	ER	PM	RE
30	9.37	9.41	0.33	7.65	7.83	2.36	5.98	6.14	2.65	5.46	5.50	0.65	4.59	4.78	4.20
70	7.08	7.07	−0.11	6.33	5.82	−8.18	5.08	4.71	−7.17	4.08	4.12	1.02	4.06	3.63	−10.75
100	6.42	6.27	−2.32	5.13	5.13	−0.07	4.30	4.22	−1.96	3.89	3.65	−6.17	3.39	3.23	−4.81
140	5.62	5.60	−0.38	4.36	4.56	4.43	3.71	3.80	2.31	3.26	3.26	−0.17	2.72	2.89	6.11
180	5.01	5.15	2.75	4.02	4.17	3.91	3.30	3.51	6.46	2.82	2.99	5.96	2.41	2.66	10.36

ER: Experimental Result, unit: $\times 10^{-12}$ m²/s; PM: Prediction Model, unit: $\times 10^{-12}$ m²/s; RE: Relative Error, %.

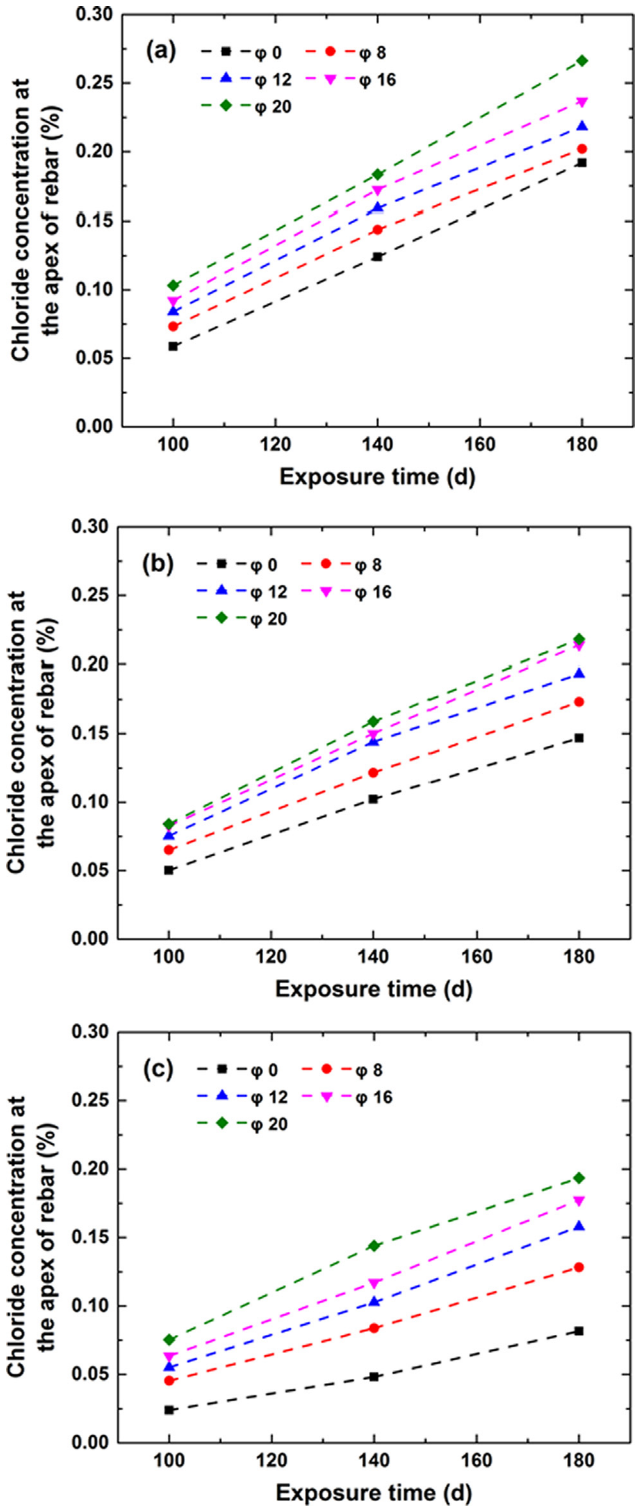

Fig. 11. Comparison of the experimental chloride concentrations at the apex of rebar: (a) $v = 0$; (b) $v = 0.2$; (c) $v = 0.4$.

where $D_{28}(A_{rc(t)})$ is the reference chloride diffusion coefficient considering the indirect blocking effect of rebar (m^2/s), and $D_{28}(A_{rc(t)}) = D_0 \cdot f(A_{rc(t)})$ by means of Eq. (5); $D_{28}(A_{pc})$ denotes the reference chloride diffusion coefficient of plain concrete (no rebar) (m^2/s), i.e. $D_{28}(A_{pc}) = D_{28}(v)$. For this paper's study, the steel bar, which embedded in concrete, would affect the content and distribution of coarse aggregate around the reinforcement; as a result, alter

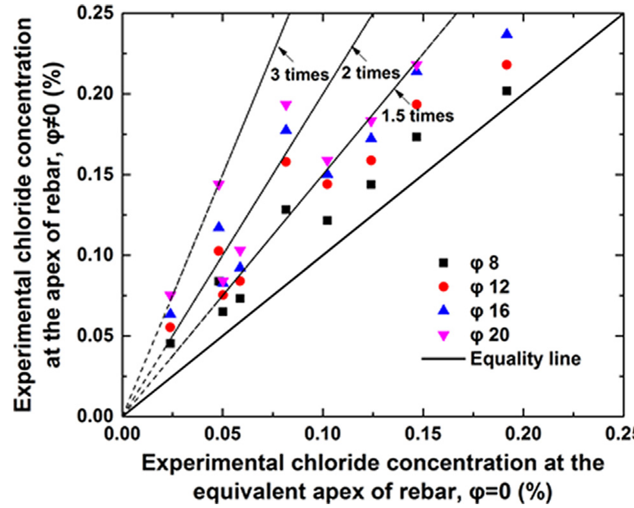

Fig. 12. Comparison of the experimental chloride concentrations at the apex of rebar ($\Phi \neq 0$) versus those of $\Phi = 0$.

the chloride diffusion coefficient at this front area of rebar. Accordingly, the indirect blocking effect coefficient of rebar in Eq. (8) is defined based on the relationship of chloride diffusion coefficient in front of steel reinforcement between the rebar presences and disappear, and the indirect blocking effect coefficient is used to quantify the effect of coarse aggregate content variation within the front area of rebar on chloride diffusion coefficient at this area in Eq. (8).

Substituting the tested average values of $A_{rc}(t)$ and A_{pc} (or v) into Eq. (8), the scatters of indirect blocking effect coefficient of rebar with various volume fractions of coarse aggregate are calculated, and these results are fitted by the linear function, as shown in Fig. 17. Ultimately, the empirical formula of indirect blocking effect coefficient of rebar ($\Phi = 16$ mm) considering the volume fraction of coarse aggregate $\alpha(v)$ is obtained using the regression analysis and expressed as:

$$\alpha(v) = 1 + 0.9416 \cdot v \tag{9}$$

(3) Prediction model of chloride concentration at the apex of rebar ($\Phi = 16$ mm) considering the volume fraction of coarse aggregate and indirect blocking effect of rebar

Uniting the Eqs. (8) and (9), the expression of $D_{28}(A_{rc(t)})$ can be determined as:

$$D_{28}(A_{rc(t)}) = \alpha(v) \cdot D_{28}(v) = (1 + 0.9416 \cdot v) \cdot D_{28}(v) \tag{10}$$

Substituting the $D_{28}(A_{rc(t)}) = \alpha(v) \cdot D_{28}(v)$ into Eq. (7) to replace the original parameter $D_{28}(v)$, the prediction model of chloride concentration at the apex of steel bar ($\Phi = 16$ mm) considering the volume fraction of coarse aggregate and indirect blocking effect of rebar is subsequently established as:

$$\begin{cases} C(x,t,v) = C_s(t) \cdot \left[1 - \mathrm{erf}\left(\dfrac{x}{2\sqrt{\frac{\alpha(v) \cdot D_{28}(v)}{1-m}\left(\frac{t_{28}}{t}\right)^m t}}\right)\right] \\ C_s(t) = 0.6009 \cdot \ln(t) - 1.6192 \\ \alpha(v) = 1 + 0.9416 \cdot v \\ D_{28}(v) = f(v) \cdot D_{28}(v=0), \quad f(v) = 1 - 1.0182 \cdot v \\ D_{28}(v=0) = 6.423 \times 10^{-12}\,\mathrm{m^2/s}, \quad m = 0.333 \end{cases} \tag{11}$$

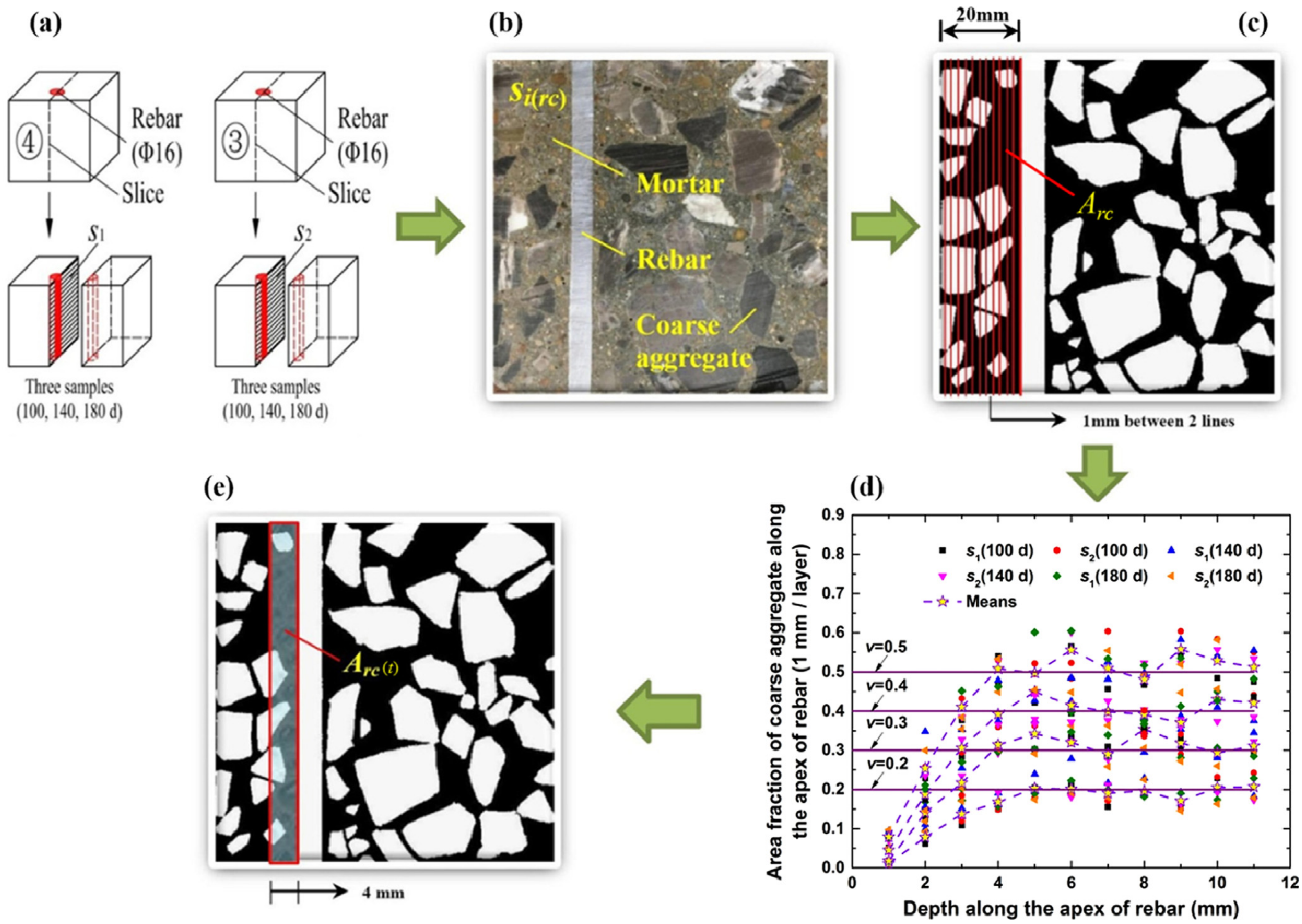

Fig. 13. Experimental procedure for determining the area fraction of coarse aggregate at the apex of rebar (Φ = 16 mm).

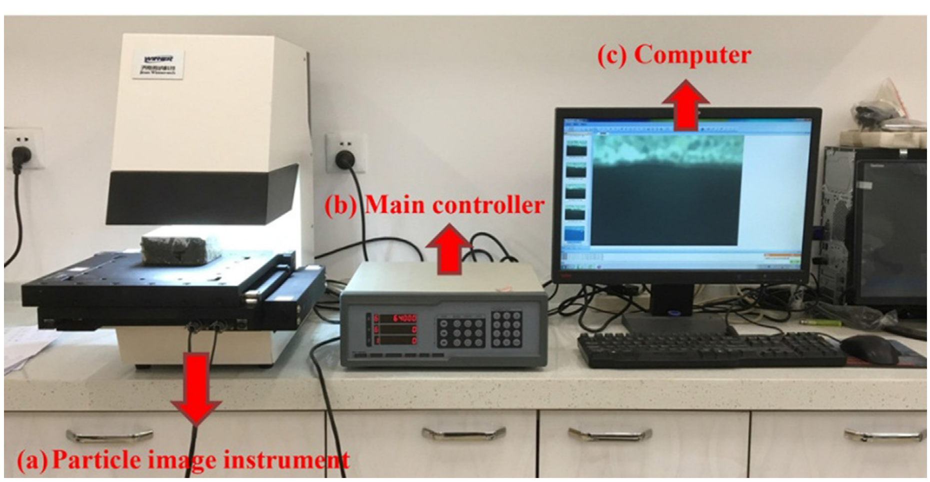

Fig. 14. Experimental device for quantifying the indirect blocking effect of rebar: (a) particle image instrument; (b) main controller; (c) computer.

Using the prediction model Eq. (11) to estimate the chloride concentrations at the apex of rebar with various volume fractions of coarse aggregate at the exposure times of 100, 140, and 180 d, the chloride results at the apex of steel bar evaluated by Eq. (11) are compared with those of experiment, as exhibited in Fig. 18. Fig. 18 illustrates the predicted chloride concentrations by model Eq. (11) are all lower than the experimental measurements, and this variation can be more significantly observed in Fig. 19. It is because that the prediction model of Eq. (11) only take account of the influences of coarse aggregate volume fraction and indirect blocking effect of steel reinforcement, whereas the direct blocking effect of steel bar is not considered in Eq. (11). Accordingly, the chloride concentrations predicted by Eq. (11) (curves in Fig. 18) are not matched with the experimental results (scatters in

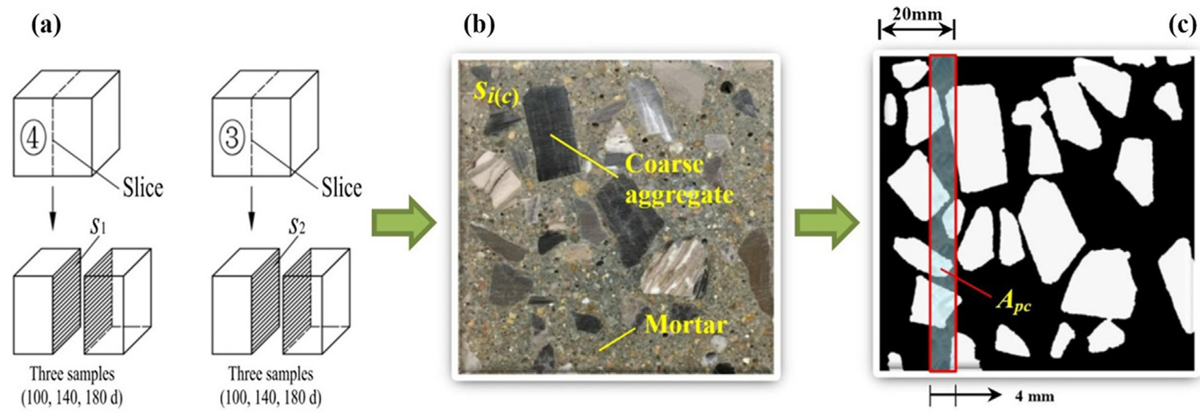

Fig. 15. Experimental procedure for determining the area fraction of coarse aggregate at the consistent influence region of steel reinforcement in plain concrete specimens.

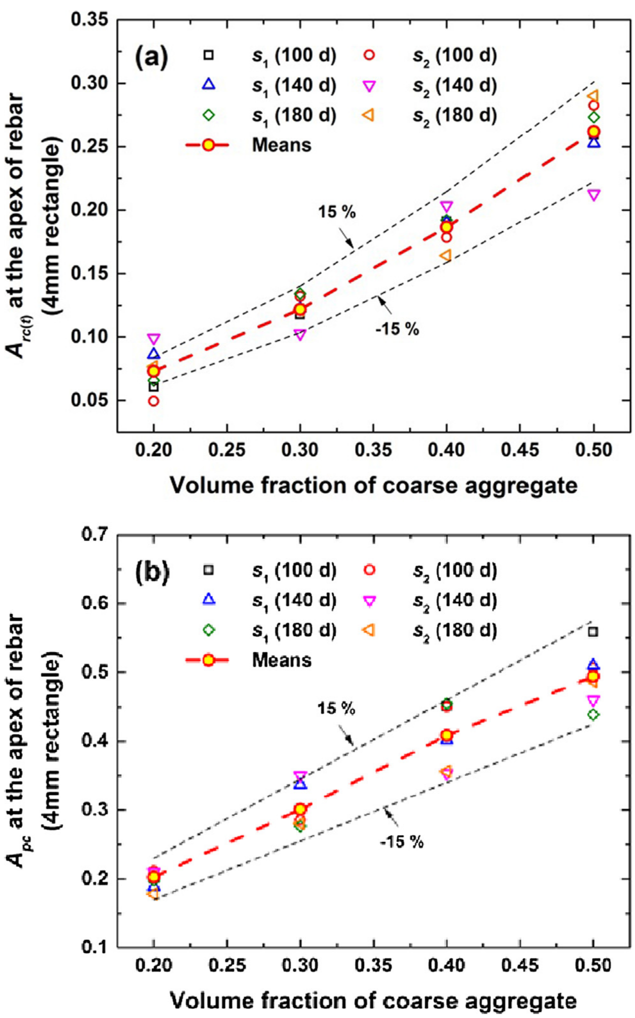

Fig. 16. Tested area fractions of coarse aggregate ($4 \times 100\,\mathrm{mm}^2$ rectangle) in (a) reinforced concrete and (b) plain concrete samples.

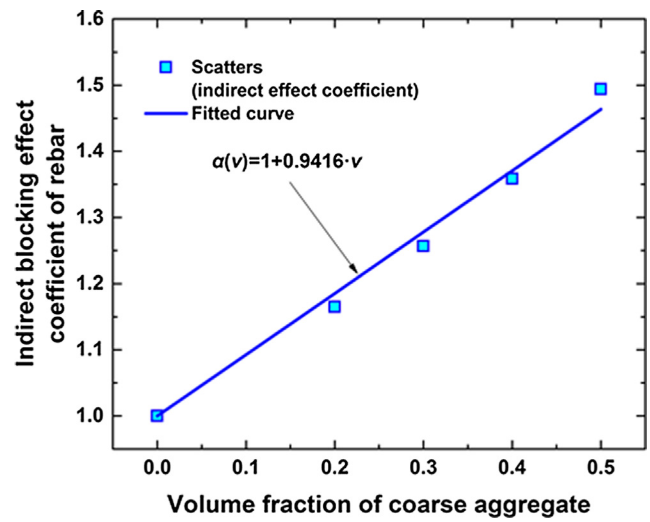

Fig. 17. Fitted curve of indirect blocking effect coefficient of rebar (Φ = 16 mm) considering the volume fraction of coarse aggregate.

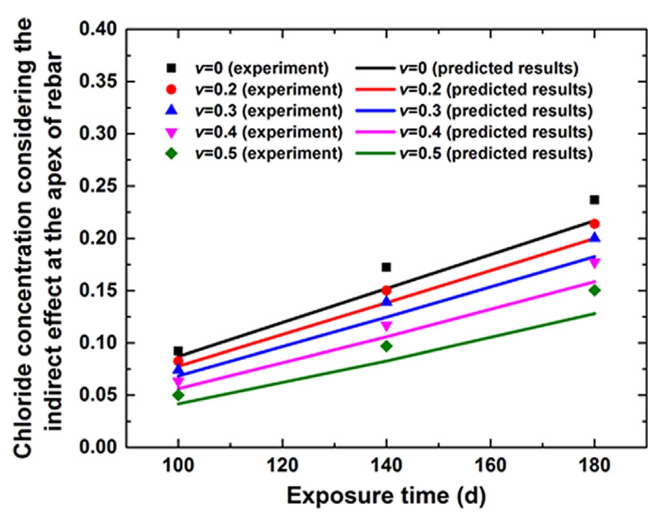

Fig. 18. Comparison of the chloride results at the apex of rebar (Φ = 16 mm): chloride concentrations with various volume fractions of coarse aggregate versus exposure time.

Fig. 18). To more accurately predict the chloride concentrations at the apex of steel reinforcement, the influence of direct blocking effect of rebar on chloride diffusion in concrete requires to be further considered.

(4) Direct blocking effect coefficient of rebar β

Comparing to the irregular shape and random distribution of coarse aggregates, the steel reinforcement can be assumed as a kind of special cylindrical aggregate with relatively fixed position

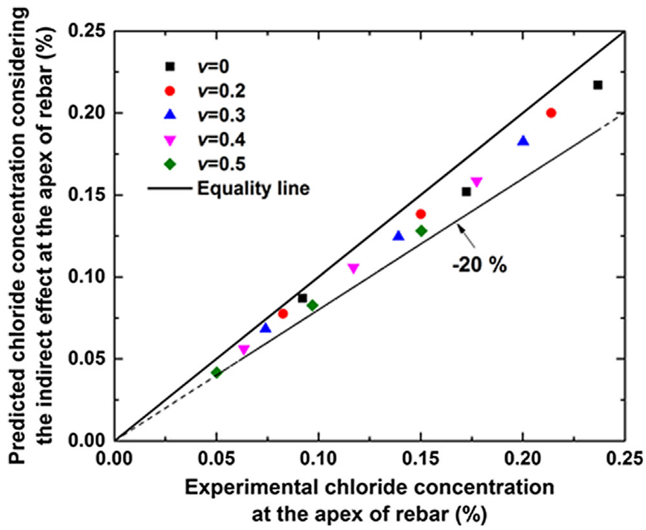

Fig. 19. Comparison of the chloride results at the apex of rebar (Φ = 16 mm): predicted chloride concentrations considering the indirect blocking effect of rebar versus the experimental measurements.

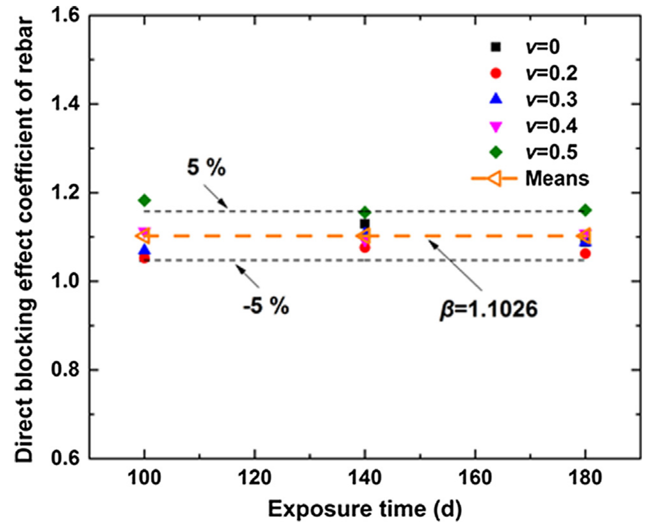

Fig. 20. Direct blocking coefficient of rebar in reinforced concrete specimens.

embedded in concrete. The transportation of chloride irons can be postulated to bypass instead of piercing through the steel bar due to the higher hardness and density of steel bar than mortar. Accordingly, the steel bar can be treated as a physical obstruction to directly block chloride ions transport in concrete resulting in the chloride concentrations accumulation at the apex of rebar, and this phenomenon is considered as the direct blocking effect of rebar [26]. On the basis of this mechanism, the ratio between the experimental chloride concentrations at the apex of rebar and the calculated chloride results by prediction model of Eq. (11) is used to define the direct blocking effect coefficient of rebar to further quantify the influence of direct blocking effect of reinforcement on chloride diffusion behaviors. The direct blocking effect coefficient of rebar (Φ = 16 mm as an instance) β is hence expressed as:

$$\beta(v,t) = C_e(c,t,v,\Phi16)/C_m(c,t,v,\Phi16) \tag{12}$$

where $C_e(c,t,v,\Phi16)$ denotes the experimental chloride concentrations at the apex of rebar (Φ = 16 mm) (%), as shown in Fig. 18 (scatters); $C_m(c,t,v,\Phi16)$ is the predicted chloride results considering the indirect blocking effect of rebar (estimated by Eq. (11)) (%), as shown in Fig. 18 (continuous lines); c is the thickness of concrete cover (mm), and other parameters are the same to above.

The direct blocking effect coefficient of rebar (Φ = 16 mm) $\beta(v, t)$ can be determined by substituting the values of $C_e(c,t,v,\Phi16)$ and $C_m(c,t,v,\Phi16)$ within Fig. 18 into Eq. (12), and the $\beta(v, t)$ results are shown in Fig. 20. Fig. 20 depicts that the direct blocking effect coefficients of rebar β are independent of coarse aggregate volume fraction and exposure time, consequently, the average value of β, i.e. $\beta = 1.1026$, is obtained and treated as the representative to quantify the direct blocking effect of rebar.

The chloride concentrations at the apex of rebar considering the volume fraction of coarse aggregate, indirect and direct blocking effects of rebar (Φ = 16 mm) can be quantified by the equivalent relationship of $C(c,t,v,\Phi16) = \beta\cdot C_m(c,t,v,\Phi16)$ in terms of Eq. (12). Thus, the prediction model of chloride concentration at the apex of steel bar (Φ = 16 mm) considering the volume fraction of coarse aggregate, indirect and direct blocking effects of rebar is established by inserting the direct blocking effect coefficient β into Eq. (11) and hence expressed as follows:

$$\begin{cases} C(x,t,v,\Phi16) = \beta\cdot C_s(t)\cdot\left[1-\mathrm{erf}\left(\dfrac{x}{2\sqrt{\frac{\alpha(v)\cdot D_{28}(v)}{1-m}\left(\frac{t_{28}}{t}\right)^m t}}\right)\right] \\ \beta = 1.1026 \\ C_s(t) = 0.6009\cdot\ln(t) - 1.6192 \\ \alpha(v) = 1 + 0.9416\cdot v \\ D_{28}(v) = f(v)\cdot D_{28}(v=0), \quad f(v) = 1 - 1.0182\cdot v \\ D_{28}(v=0) = 6.423\times10^{-12}\mathrm{m}^2/\mathrm{s}, \quad m = 0.333 \end{cases} \tag{13}$$

Fig. 21 exhibits the comparison between the chloride concentrations at the apex of rebar (Φ = 16 mm) predicted by Eq. (13) and the experimental results for reinforced concrete with various volume fractions of coarse aggregate at different exposure times. The magnitudes of the chloride concentrations at the apex of rebar evaluated by the prediction model Eq. (13) are in good agreement with those from the experiments. Also, the chloride concentrations evaluated by Eq. (13) versus those of experiment are plotted in

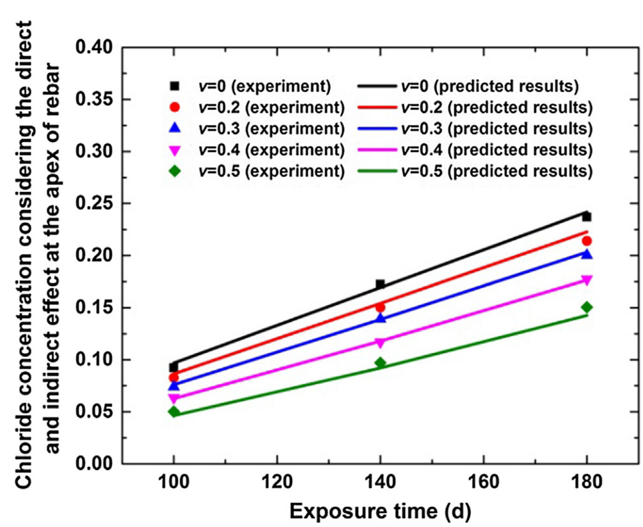

Fig. 21. Comparison of the chloride results at the apex of rebar (Φ = 16 mm): chloride concentrations with various volume fractions of coarse aggregate versus exposure time.

Fig. 22. This drawn shows that most of the scatters fall approximately on the equality line and within a ±5% relative error margin, validating the accuracy and reasonability of the prediction model of Eq. (13) developed in this paper.

(5) Improved direct blocking effect coefficient of rebar $\beta_r(\Phi/c)$

The aforementioned conclusions are all derived and determined on the precondition of the steel bar diameter Φ = 16 mm. However, the experimental chloride concentrations at the apex of rebar increase with the diameter of steel bar Φ increasing. To more widespread application of this paper's proposed prediction model considering the effects of coarse aggregate and steel reinforcement, the tested chloride concentrations at the apex of rebar for reinforced concrete specimens with the diameter of rebar Φ = 16 mm and various volume fractions of coarse aggregate are treated as the base values to improve the direct blocking effect coefficient of rebar, and then, to quantify and determine the direct blocking effect coefficient of rebar with different diameters. To sum up, the normalized chloride concentrations at the apex of rebar C_n are defined and expressed as:

$$C_n(c,t,v,\Phi) = C_e(c,t,v,\Phi)/C_e(c,t,v,\Phi 16) \tag{14}$$

where $C_e(c,t,v,\Phi)$ is the tested values of chloride concentration at the apex of rebar for different reinforced concrete specimens, in which includes the diameters of steel bar Φ = 8, 12, 16, 20 mm and the volume fractions of coarse aggregate v = 0, 0.2, 0.3, 0.4, and 0.5; The other parameters are consistent to above. Substituting the corresponding experimental chloride concentrations at the apex of rebar into Eq. (14), the normalized chloride concentrations at the apex of rebar for reinforced concrete specimens with various volume fractions of coarse aggregate against the diameters of steel reinforcement are calculated and shown in Fig. 23.

Fig. 23 illustrates that the relative errors between the scatters of normalized chloride concentrations at the apex of rebar, $C_n(c,t,v,\Phi)$, and their average values are almost within ±5% range when the diameter of rebar is constant. Consequently, it's appropriate to consider that the values of C_n are independent of coarse aggregate volume fraction and exposure time. Accordingly, the average values of C_n at each diameter are used as the representatives, and the linear function is applied to fit the relationship between the C_n and the normalized rebar diameter Φ/c, as shown in Fig. 23 (where c means the thickness of concrete cover). Finally, the improved direct blocking effect of rebar is hence expressed as follows:

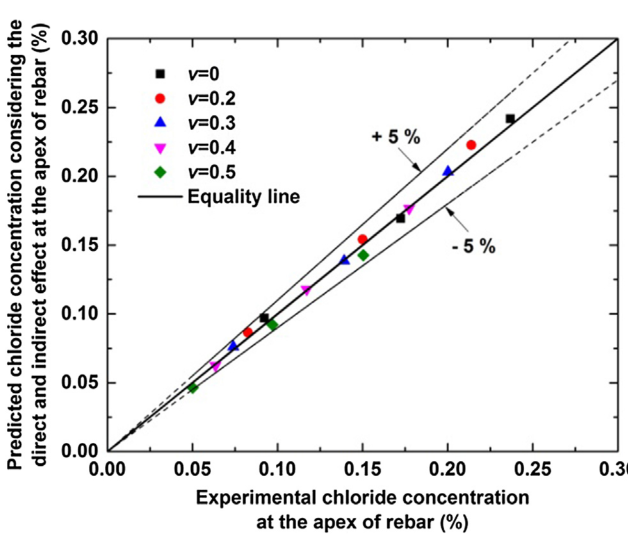

Fig. 22. Comparison of the chloride results at the apex of rebar (Φ = 16 mm): predicted chloride concentrations considering the direct and indirect blocking effects of rebar versus the experimental measurements.

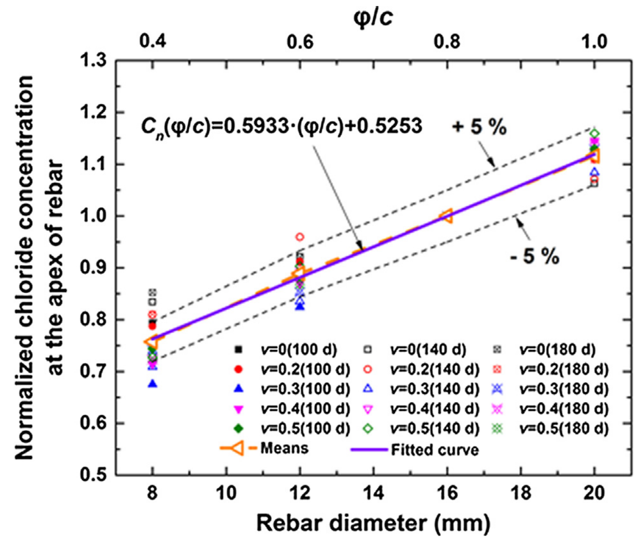

Fig. 23. Means of normalized chloride concentrations at the apex of rebar in reinforced concrete specimens versus rebar diameter and the fitted curve of $C_n(\Phi/c)$.

$$\beta_r\left(\frac{\Phi}{c}\right) = \beta \cdot C_n\left(\frac{\Phi}{c}\right) = 0.5933 \cdot \left(\frac{\Phi}{c}\right) + 0.5253 \tag{15}$$

(6) Prediction model of chloride concentration at the apex of rebar considering the coupling effects of coarse aggregate and steel reinforcement

Using the improved direct blocking effect coefficient $\beta_r(\Phi/c)$ expressed in Eq. (15) to replace the original β within Eq. (13), the prediction model of chloride concentration at the apex of rebar considering the coupling effects of coarse aggregate and steel reinforcement is ultimately established and expressed as:

$$\begin{cases} C(x,t,v,\Phi) = \beta_r\left(\frac{\Phi}{c}\right)\cdot C_s(t)\cdot\left[1-\mathrm{erf}\left(\frac{x}{2\sqrt{\frac{\alpha(v)\cdot D_{28}(v)}{1-m}\left(\frac{t_{28}}{t}\right)^m t}}\right)\right] \\ \beta_r\left(\frac{\Phi}{c}\right) = 0.5933\cdot\left(\frac{\Phi}{c}\right)+0.5253 \\ C_s(t) = 0.6009\cdot\ln(t) - 1.6192 \\ \alpha(v) = 1 + 0.9416\cdot v \\ D_{28}(v) = f(v)\cdot D_{28}(v=0), \quad f(v) = 1 - 1.0182\cdot v \\ D_{28}(v=0) = 6.423\times 10^{-12}\,\mathrm{m^2/s}, \quad m = 0.333 \end{cases} \tag{16}$$

Similarly, the chloride concentrations at the apex of rebar tested by experiment are compared with the results estimated by the proposed prediction model Eq. (16), as shown in Fig. 24. Fig. 24 exhibits that the magnitudes of the chloride concentrations at the apex of rebar evaluated by prediction model Eq. (16) are in good agreement with those from the experiments. Moreover, the chloride results for various reinforced concrete specimens predicted by means of the model Eq. (16) against the experimental measurements are plotted in Fig. 25. This figure shows that almost all of the chloride concentrations at the apex of rebar estimated by the prediction model Eq. (16) are located within a ±15% error margin, validating the accuracy and reliability of the prediction models for reinforced concrete specimens proposed in this paper. To sum up, the prediction model of chloride concentration at the apex of rebar considering the coupling effects of coarse aggregate and steel reinforcement (Eq. (16)) can accurately predict the chloride con-

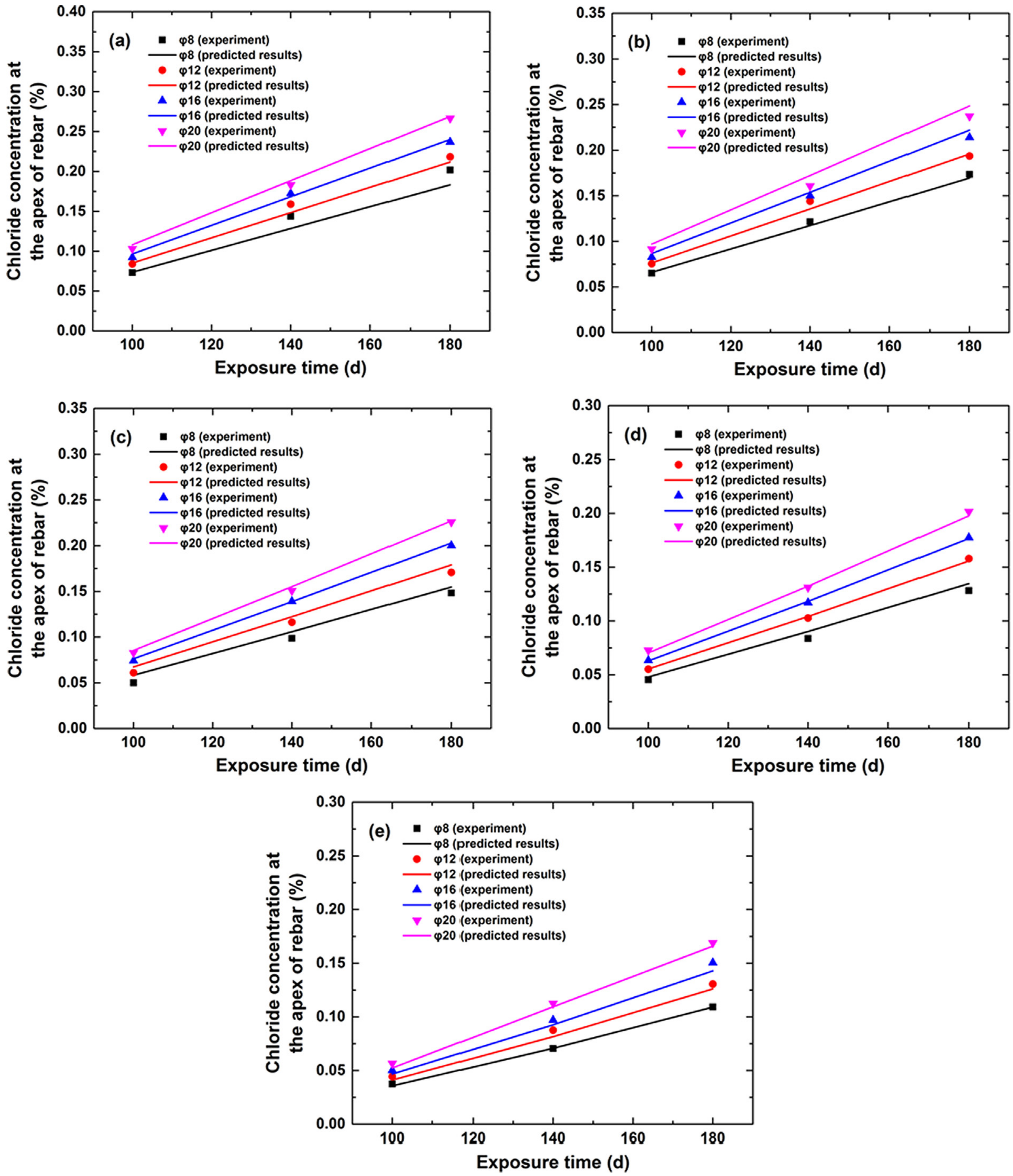

Fig. 24. Comparison of the chloride concentrations at the apex of rebar in reinforced concrete between experiment and prediction model of Eq. (12): (a) $v = 0$; (b) $v = 0.2$; (c) $v = 0.3$; (d) $v = 0.4$; (e) $v = 0.5$.

centrations at the apex of rebar with different coarse aggregate volume fractions and diameters of steel bar at arbitrary exposure times.

4. Conclusions

For this paper's study, an in-door physical experiment for chloride diffusion in plain and reinforced concrete specimens exposed to marine tidal environment was carried out. The specimens were cast using different volume fractions of coarse aggregate and diameters of steel reinforcement. The chloride concentrations for experimental specimens were measured at various exposure times, and they were adopted to further investigate the common influences of coarse aggregate volume fraction and blocking effect of rebar on chloride diffusion in concrete. Finally, a prediction model of chloride diffusion in concrete considering the coupling effects of coarse aggregate and steel reinforcement was proposed. The following significant conclusions are showed as:

(1) An in-door experiment for chloride diffusion in plain concrete specimens with different volume fractions of coarse aggregate exposed to marine tidal zone was carried out,

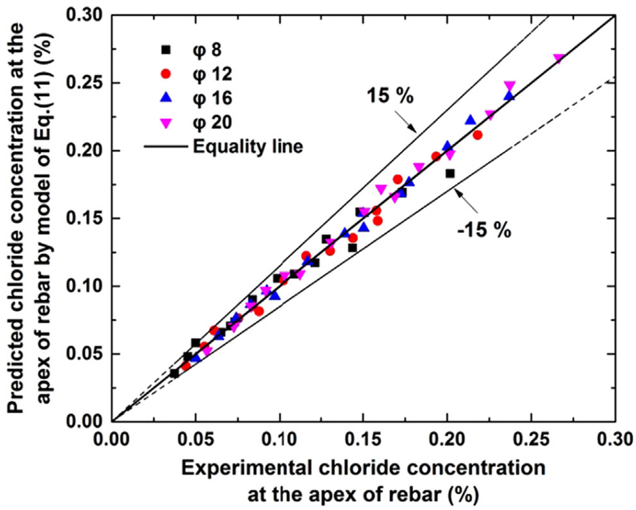

Fig. 25. Comparison of the chloride concentrations at the apex of rebar by the prediction model of Eq. (12) versus those of experiment in reinforced concrete specimens.

and the chloride profiles at various exposure times were tested. The variations for surface chloride concentration and apparent chloride diffusion coefficient versus exposure time are obtained by fitting the Fick's second law of diffusion to the experimental chloride profiles using the regression analysis. The conclusions indicated that the surface chloride concentration is independent of coarse aggregate effects, nevertheless, the apparent chloride diffusion coefficients decreased with the exposure time increasing.

(2) The impact factor of coarse aggregate volume fraction $f(v)$ was proposed to quantify the effect of coarse aggregate on chloride diffusion coefficient. The $f(v)$ was adopted to improve the chloride diffusion coefficient within the analytical solution of Fick's second law. A prediction model of chloride diffusion profiles in concrete considering the effect of coarse aggregate volume fraction was established and the accuracy of this model was validated using the experimental chloride results.

(3) An in-door physical experiment for chloride diffusion in reinforced concrete specimens exposed to marine tidal environment was carried out. The specimens were cast using various volume fractions of coarse aggregate and diameters of steel reinforcement. The chloride concentrations for experimental specimens at different positions and exposure times were tested. According to the experimental measurements, it can be found that the chloride concentrations at the apex of rebar were greater than those of other positions, which indicated that the blocking effect of steel bar can significant enhance the chloride concentrations at the surface of rebar. The steel reinforcement embedded in concrete can alter the meso-scopic structure of concrete adjacent to the rebar, i.e. update (decrease) the coarse aggregate content and distribution within a region of $4 \times 100\ mm^2$ rectangle in front of the steel reinforcement, thereby, affect (increase) the chloride diffusion coefficient at this area of rebar, which meant the indirect blocking effects of rebar. Moreover, the steel bar was regarded as a physical obstruction to block chloride ions diffusion in concrete resulting in the chloride concentrations accumulation at the apex of rebar, which denoted the direct blocking effect of rebar.

(4) The indirect and direct blocking effect coefficients $\alpha(v)$, $\beta_r(\Phi/c)$ were proposed to quantify the influence of blocking effect of steel reinforcement on chloride concentrations at the apex of rebar. Substituting the $\alpha(v)$ and $\beta_r(\Phi/c)$ in the prediction model of chloride diffusion in concrete considering the volume fraction of coarse aggregate, an improved prediction model of chloride concentration at the apex of rebar considering the coupling effects of coarse aggregate and steel reinforcement was established. The accuracy and reasonability for this paper's proposed prediction model were validated using the experimental measurements.

Conflicts of interest

None.

Acknowledgments

The authors would like to appreciate the insightful and constructive comments of two anonymous reviewers. This research was supported by the National Key Research and Development Program of China (2016YFC0802204, 2016YFC0802201), the National Natural Science Foundation of China (51679166), the National Natural Science Fund for Innovative Research Groups Science Foundation (51321065), and the Construction Science and Technology Project of the Ministry of Transport of the People's Republic of China (2014328224040).

References

[1] A. Costa, J. Appleton, Case studies of concrete deterioration in a marine environment in Portuga, Cement. Concrete. Comp. 24 (1) (2002) 169–179.
[2] Y.D. Yan, W.L. Jin, J. Chen, Experiments of chloride ingression in flexural reinforced concrete beams, Adv. Struct. Eng. 15 (2) (2012) 277–286.
[3] S.L. Amey, D.A. Johnson, M.A. Miltenberger, Predicting the service life of concrete marine structures: an environmental methodology, ACI. Struct. J. 95 (2) (1998) 205–214.
[4] F.H. Wittmann, Structure of concrete with respect to crack formation, Fracture Mech-anics of Concrete, Elsevier, London/New York, 1983, pp. 43–74.
[5] C.C. Yang, S.W. Cho, Approximate migration coefficient of percolated interfacial transition zone by using the accelerated chloride migration test, Cem. Concr. Res. 35 (2) (2005) 344–350.
[6] C.C. Yang, Effect of the percolated interfacial transition zone on the chloride migration coefficient of cement-based materials, Mater. Chem. Phys. 91 (2) (2005) 538–544.
[7] S.P. Shah, High Performance Concrete: Past, present and future, Proc., Int. Symp. on High Performance Concrete: Workability, Strength and Durability. C. K. Leung, Y. Z. Li, and J. T. Ding, eds., Vol. 1, Hong Kong Univ. of Science and Technology, Hong Kong. (2000) 3–29.
[8] S.D. Abyaneh, H.S. Wong, N.R. Buenfeld, Modelling the diffusivity of mortar and concrete using a three-dimensional mesostructure with several aggregate shapes, Comput. Mater. Sci. 78 (1) (2013) 63–73.
[9] X.X. Li, Y. Xu, S. Chen, Computational homogenization of effective permeability in three-phase mesoscale concrete, Constr. Build. Mater. 121 (2016) 100–111.
[10] Y.Z. Wang, C.X. Liu, Y.C. Wang, Q.M. Li, H. Liu, Time-and-depth-dependent model of chloride diffusion coefficient for concrete members considering the effect of coarse aggregate, J. Mater. Civ. Eng. 30 (3) (2018). 04017302 (1-12). 10.1061/(ASCE)MT.1943-5533.0002161.
[11] Y.Z. Wang, L.J. Wu, Y.C. Wang, Q.M. Li, Z. Xiao, Prediction model of long-term chloride diffusion into plain concrete considering the effect of the heterogeneity of materials exposed to marine tidal zone, Constr. Build. Mater. 159 (2018) 297–315.
[12] Y.Z. Wang, L.J. Wu, Y.C. Wang, C.X. Liu, Q.M. Li, Effects of coarse aggregates on
[13] Corrosion Propagation of Carbon Steel Rebars in High Performance Concrete, Francisco J Presuel-Moreno, Rolando Bencosme, Kazi Hoque, Manzural Nazim, Amirkhosro Kazemi, Fujian Tang, 2018/11
[14] Corrosion Prevention of Bridge Tendons using Flexible Filler Materials, Francisco J Presuel-Moreno, Carlos Castaneda, Ingrid Santillan, Amirkhosro Kazemi, Fujian Tang, 2018/11
[15] Chloride Diffusivity and Resistivity of Cured and Mature Binary/ Ternary Concrete. Francisco J Presuel-Moreno, Sanjoy Barman, Farhad Raof, Amirkhosro Kazemi, 2019/2.

[18] JTJ 202-2011: 2011. Specifications for concrete construction of port and waterway engineering. Ministry of transport of the people's republic of China, Beijing, 2011 (in Chinese).
[19] L.Y. Li, J. Xia, S.S. Lin, A multi-phase model for predicting the effective diffusion coefficient of chlorides in concrete, Constr. Build. Mater. 26 (1) (2012) 295–301.
[20] GB 50164-2011:2011. Standard for quality control of concrete. Ministry of Housing and Urban-Rural Development of the people's republic of China, Beijing, 2011 (in Chinese).
[21] C. Xu, W.L. Jin, Z.Y. Li, A new test method to simulate chloride penetration into concrete in tidal zone, The Ocean Eng. 29 (4) (2011) 51–59 (in Chinese).
[22] JTJ 270-98: 1998. Testing code of concrete for port and waterway engineering. Ministry of transport of the people's republic of China, Beijing, 1998 (in Chinese).
[23] F.H. Xiang, Study on the Transport Mechanism of Chloride ions in Concrete, Central South University, Changsha, HN, China, 2011 (in Chinese).
[24] L. Pang, Q. Li, Service life prediction of RC structures in marine environment using long term chloride ingress data: comparison between exposure trials and real structure surveys, Constr. Build. Mater. 113 (2016) 979–987.
[25] M. Collepardi, A. Marcialis, R. Turriziani, Penetration of chloride ions into cement paste and concrete, J. Am. Ceram. Soc. 10 (55) (1972) 534–535.
[26] M.D.A. Thomas, P.B. Bamforth, Modelling chloride diffusion in concrete effect of fly ash and slag, Cement. Concrete. Res. 29 (4) (1999) 487–495.
[27] L.J. Wu, W. Li, X.N. Yu, Time-dependent chloride penetration in concrete in marine environments, Constr. Build. Mater. 167 (2017) 406–413.
[28] Z.Q. Jin, X. Zhao, T.J. Zhao, J.Q. Li, Chloride ions transportation behavior and binding capacity of concrete exposed to different marine corrosion zones, Constr. Build. Mater. 177 (2018) 170–183.
[29] J.Q. Wu, P.P.N. Faye, W.M. Zhang, B. Diao, Chloride diffusivity and service life prediction of RC columns with sustained load under chloride environment, Constr. Build. Mater. 158 (2018) 97–107.
[30] J.Z. Zhang, J. Zhao, Y.R. Zhang, Y.H. Gao, Y.Y. Zheng, Instantaneous chloride diffusion coefficient and its time dependency of concrete exposed to a marine tidal environment, Constr. Build. Mater. 167 (2018) 225–234.
[31] A. Petcherdchoo, Time dependent models of apparent diffusion coefficient and surface chloride for chloride transport in fly ash concrete, Constr. Build. Mater. 38 (1) (2013) 497–507.
[32] L. Tang, J. Gulikers, On the mathematics of time-dependent apparent chloride diffusion coefficient in concrete, Cement. Concrete. Res. 37 (2007) 589–595.
[33] H. Song, C. Lee, K.Y. Ann, Factors influencing chloride transport in concrete structures exposed to marine environments, Cement. Concrete. Comp. 30 (2) (2008) 113–121.
[34] A. Farahani, H. Taghaddos, M. Shekarchi, Prediction of long-term chloride diffusion in silica fume concrete in a marine environment, Cement. Concrete. Comp. 59 (2015) 10–17.
[35] H. Yu, R.J. Himiob, W.H. Hartt, Effects of reinforcement and coarse aggregates on chloride ingress into concrete and time-to-corrosion: Part 1—Spatial Chloride Distribution and Implications, Corrosion. 63 (9) (2007) 843–849.
[36] H. Yu, R.J. Himiob, W.H. Hartt, Effects of reinforcement and coarse aggregates on chloride ingress into concrete and time-to-corrosion: Part 2—Spatial Distribution of Coarse Aggregates, Corrosion. 63 (10) (2007) 924–931.
[37] J.J. Zheng, C.Q. Li, L.Y. Zhao, Simulation of two-dimensional aggregate distribution with wall effect, ASCE-J. Mater. Civil. Eng. 15 (5) (2003) 506–510.
[38] W.X. Xu, H.S. Chen, Influences of shapes and sizes of aggregates on wall effect of concrete, J. Chin. Ceram. Soc. 39 (9) (2011) 1498–1504 (in Chinese).
[39] W.X. Xu, H.S. Chen, Influence of size distribution of multiscale elliptical aggregates on wall effect of concrete, J. Southeast Univ. (Natural Science Edition). 41 (5) (2011) 1048–1053 (in Chinese).